RIGA TECHNICAL UNIVERSITY
1862

Vlads Vladinovskis

RESEARCH AND DEVELOPMENT OF 3D PRINTING EQUIPMENT FOR THE MANUFACTURE OF ORTHOPEDIC REHABILITATION PRODUCTS

Summary of the Doctoral Thesis

RIGA TECHNICAL UNIVERSITY

Faculty of Computer Science, Information Technology and Energy
Institute of Industrial Electronics and Electrical Engineering

Vlads Vladinovskis

Doctoral Student of the Study Program "Computerized Control of Electrical Technologies"

RESEARCH AND DEVELOPMENT OF 3D PRINTING TECHNOLOGIES FOR THE PRODUCTION OF ORTHOPEDIC REHABILITATION PRODUCTS

Summary of the Doctoral Thesis

Scientific supervisor
Professor Dr. sc. ing.
IĻJA GALKINS

RTU Press
Riga 2024

DOCTORAL THESIS PROPOSED TO RIGA TECHNICAL UNIVERSITY FOR PROMOTION TO THE SCIENTIFIC DEGREE OF DOCTOR OF SCIENCE

To be granted the scientific degree of Doctor of Sciences (Ph. D.), the present Doctoral Thesis has been submitted for defense at the open meeting of the RTU Promotion Council on October 23, 2024 at 15.00 at the Faculty of Electrical and Environmental Engineering of Riga Technical University, 12/1 Āzenes Street, Room 525.

OFFICIAL REVIEWERS

Professor Dr. sc. ing. Nadežda Kuņicina,
Riga Technical University

Associate Professor Dr. sc. ing. Vladimir Kuts,
Tallinn University of Technology, Estonia

Associate Professor Dr. sc. ing. Andrei Lobov,
Norwegian University of Science and Technology, Norway

DECLARATION OF ACADEMIC INTEGRITY

I hereby declare that the Doctoral Thesis submitted for review to Riga Technical University for promotion to the scientific degree of Doctor of Science (Ph.D.) is my own. I confirm that this Doctoral Thesis has not been submitted to any other university for promotion to a scientific degree.

Vlads Vladinovskis ……………………………. (signature)
Date: ………………………

The Doctoral Thesis has been written in Latvian. It consists of a Summary, 88 figures, 13 tables, and 3 appendices; the total number of pages is 111. The Bibliography contains 84 titles.

ACKNOWLEDGMENTS

First and foremost, I would like to express my deepest gratitude and respect to my PhD supervisor, Professor Iļja Galkins, for his invaluable support, guidance, and professional advice throughout the development of my thesis. His expertise, recommendations, and dedicated time greatly contributed to the quality of my work and facilitated my growth in both academic and professional fields. Professor Galkins' support and encouragement have been indispensable.

I would also like to extend my special thanks to my colleagues from the Institute of Industrial Electronics and Electrical Engineering. Your professional advice, technical assistance, and friendly support were crucial throughout this journey. Your collegiality and spirit of cooperation helped overcome challenges and achieve the set goals. I am very grateful to have had the opportunity to work alongside such knowledgeable and supportive individuals.

I also thank the reviewers of my thesis for their valuable comments, critique, and recommendations, which contributed to the improvement and refinement of my work. Your professional insights and objectivity helped to better identify and enhance the essential aspects of the thesis.

Finally, I am especially grateful to Mg. sc. ing. Nika Ijudina for her unwavering support, invaluable advice, and indispensable assistance throughout the entire development of the thesis. Her encouragement and motivation were a significant force that helped me overcome challenges and successfully move forward.

I cannot fail to thank my family for their unwavering support, understanding, and patience during this time. Your presence and encouragement have given me the strength and resilience to continue my work and achieve my goals. Thank you from the bottom of my heart!

CONTENTS

GENERAL OVERVIEW OF THE THESIS

Topicality of the research

With the rapid development of the medical industry, the demand for personalized medicine tools that provide an individual approach to the needs of each person and promote the healing process of excavations has grown strongly. More expensive devices can be a barrier to a personalized approach, but the result is a much higher level of health care. To reduce this disadvantage, 3D printing can be used as an alternative. Creating a 3D model of a rehabilitated human limb using 3D scanning can ensure that the final printed product perfectly matches the correct anatomical shape of the body part. However, using early prediction methods, the orthosis will be able to be printed based on the expected result in the future, printing new orthoses according to the progress of rehabilitation. Products produced with 3D printing will be lighter but with better mechanical properties. So that the 3D printed product does not have seams that can rub the skin, a multi-layer non-flat cylindrical type 3D printer will be constructed, which is able to eliminate this problem.

The Thesis is aimed at expanding the boundaries of 3D printing technology by developing and implementing non-planar and cylindrical printing that can overcome the limitations of traditional layered printing. This will help advance the development of the next generation of custom orthotics and medical rehabilitation devices that better fit the patient's anatomy, improving patient comfort and performance. The work is planned to improve the energy efficiency of the printing process and reduce material waste by optimizing the CAD model slicing software and printing processes. An R&D non-planar multi-axis 3D printer prototype will incorporate advanced control techniques aimed at overcoming existing traditional 3D printing problems. Together with the development of a new method of slicing models, these advances work together to improve the quality and structural uniformity of printed objects in 3D printing.

The doctoral work has been carried out to research multi-axis non-planar and cylindrical technology and the development of a 3D printing printer, where the prototype will potentially be able to efficiently produce complex cylindrical and also free forms with better mechanical parameters without the use of support material. Development of affordable and higher functionality software based on Python code and visual 3D development environment Rhinoceros 3D is necessary in the field of 3D printing, development, and research in this field is perspective and important in the scientific environment.

Orthoses have different types of complex shapes and require the use of different types of equipment to make them. If 3D printing solutions are to be used, it is necessary to use different printers, and in order to enable the printing of orthoses within one machine, the Thesis has developed equipment and methods that realize traditional FDM printing combined with three and five-axis irregular cylindrical 3D printing.

The focus is on mitigating the delamination problems of 3D printed models by developing alternative methodologies for slicing CAD models and reorienting CAD objects in space during

model pre-production. Based on this, existing non-planar 3D printer control methods lack precision, are difficult to use, and there is no existing unified printer software.

The Doctoral Thesis describes the means of orthopaedic rehabilitation, their requirements and manufacturing process, existing 3D printing technologies applicable in medicine and the 3D printing industry, existing 3D printing problems and their possible solutions, as well as an experimental part has been created, where the stages of how this type was exhibited are described. The printer needed materials and steps. A prototype of a multi-axis non-flat cylindrical type 3D printer with the ability to switch from 3-axis mode to 5-axis mode has been created. The parameters of the prototype have also been compared, and conclusions have been drawn about the work done.

The purpose of the Thesis

The Thesis aims to develop a non-planar cylindrical 3D printing method and an FDM 3D printing machine that combines the use of traditional and cylindrical printing methods in one machine for the production of individual orthopedic rehabilitation devices. The work envisages the development and implementation of specialized software and control algorithms for cylindrical and non-planar 3D printing in order to increase the accuracy and efficiency of printing individual and personalized rehabilitation products with improved mechanical parameters compared to traditional 3D printing methods, and to develop software and a prototype of a multi-axis 3D printer to be able to more precisely control the printing process and improve the mechanical properties of the products.

The primary goal is to create a more flexible and interconnected layer structure, as well as to solve the problem of the heterogeneous composition of printed objects. Using non-planar and cylindrical methods in pattern distribution, as well as object orientation optimization in space, this research aims to significantly improve the surface quality and structural homogeneity of 3D printed objects.

Hypothesis

The surface quality and mechanical parameters of 3D printed individually customizable orthopedic rehabilitation devices can be significantly improved, as well as 3D printing itself can be significantly accelerated and reduced in cost, by means of a new method of control and preparation for non-planar FDM printing that includes:

1. step-by-step sequence of CAD models geometry changes;

2. refinement of the standard generated G-code, which combines standard open access hardware and software solutions for FDM 3D printing for preparing and slicing CAD models.

Objectives

1. Collect information found in the scientific literature on 3D printing methods and slicing methods of CAD models.
2. Investigate and propose alternative non-planar slicing methods for FDM 3D printing equipment, create an experimental stand and test the developed method.
3. Summarize the results of the experimental stand and develop a full-fledged FDM 3D prototype based on them.
4. Perform prototype improvements and realize multi-solutions for complex form FDM 3D printing.
5. Realize fast switching between traditional, three-axis cylindrical and five-axis non-planar FDM 3D printing modes and perform product testing with the technology.
6. Summarize the results and make proposals about the advantages, disadvantages, and possible improvements of the technology

Research tools and methods

Data collection and calculations were performed in the *MS Excel* environment, *Autodesk Tinkercad* was used for modeling and representation of electrical circuits, *Matlab* environment was used for data processing and visualization, *Autodesk Fusion 360* and *Solidworks 3D CAD* were used for 3D model modeling and animation, and *Ultimaker Cura* 5.2.0, *Prusa Slicer 2.7.1* and *Creality Slicer 4.8.2* was used for 3D printing model slicing and preparation. *Python* and *C++* languages were used for G-code editing and prototype control program compilation, *Autodesk AutoCAD* and *Solidworks 3D CAD* software were used for calculations and temperature simulations.

During the development and experimental part of the Doctoral Thesis, laboratory instruments and equipment of RTU IEEI laboratory and RTU Design Factory "theLAB" were used. It included various types of power supplies, a thermal camera, oscilloscopes, multimeters and other materials.

During the development of the prototype, a few different microcontroller control boards with different configurations of stepper motor drivers were used, especially several *STM32, Arduino Mega* and *Uno* and *Raspberry Pi* microcontroller boards. *Visual Code Studio,* in conjunction with *Python 3.11* and *Arduino IDE,* was used for microcontroller programming and debugging.

Novelty

1. A new step-by-step method that describes how using standard open-access hardware and software to achieve non-planar printing without specialized non-planar slicing software and hardware development.
2. A software solution that reads and edits STL CAD model geometry to use the provided method has been developed. The developed software changes the model according to the method needed to achieve printing on a rotating cylinder surface.

3. A software solution that reads traditionally sliced G-code and changes material extrusion amount to properly print on a rotating cylinder surface has been made. The software counts layer numbers and calculates each layer area to provide the proper extrusion amount for each printed layer.

4. A hardware prototype that combines three printing modes (traditional planar, 3-axis rotational cylinder non-planar, and 5-axis full non-planar) has been developed. It uses the provided printing method to implement non-planar printing by use of standard open-access software and, at the same time, effectively uses workspace.

Approbation of the Thesis

In total, six publications were developed during the studies, four of which are mentioned in the Thesis. The approbation and practical significance of the research results have been discussed in the following publications:

1. **V. Vladinovskis**, "Potential Power Management Efficiency Improvements in Desktop 3D Printers," *2022 IEEE 63rd International Scientific Conference on Power and Electrical Engineering of Riga Technical University (RTUCON)*, Riga, Latvia, 2022, pp. 1–6, doi: 10.1109/RTUCON56726.2022.9978882.

2. **V. Vladinovskis**, "Review of 3D Printing Technologies and Considerations on Their Use in Orthopedy," *2020 IEEE 61st International Scientific Conference on Power and Electrical Engineering of Riga Technical University (RTUCON)*, Riga, Latvia, 2020, pp. 1–6, doi: 10.1109/RTUCON51174.2020.9316483.

3. **V. Vladinovskis**, "Review of Lathe Type 3D Printers and Their Possible Improvements," *2021 IEEE 9th Workshop on Advances in Information, Electronic and Electrical Engineering (AIEEE)*, Riga, Latvia, 2021, pp. 1–5, doi: 10.1109/AIEEE54188.2021.9670257.

4. **V. Vladinovskis,** "Selection of microcontroller board and stepper motor driver for FDM 3D printing to reduce power consumption", *2023 IEEE 64th International Scientific Conference on Power and Electrical Engineering of Riga Technical University (RTUCON),* Riga, Latvia, 2023, pp. 1–6, doi: 10.1109/RTUCON60080.2023.10413037.

LITERATURE REVIEW

1.   ORTHOPEDIC REHABILITATION DEVICES

1.1.   Use and requirements

Orthopedics is a medical section that studies the diagnosis, prevention and rehabilitation of the human musculoskeletal system. It includes prosthetics, a discipline borrowed from prosthetic and orthotic research and fabrication. Another department of orthopedics is rehabilitation. It is a set of measures tasked with restoring a patient's lost abilities after an injury or surgery. Various types of auxiliary equipment are widely used to rehabilitate patients. Orthopedic dressings or orthoses are used to facilitate the healing process of broken bones or laces. They act as a support to hold the limbs in place and lock the bones in the correct anatomical position. Orthoses can be made of plaster, glass fiber, thermoplastic, wood or metal.

Orthoses' main requirements are to be comfortable, lightweight and durable. They must be easy to put on and take off, they must be functional and do not harm, they must have a long service life and be easy to repair.

Since 2013, 3D printing technologies have been used for the production of today's orthoses, and various companies have been using this technology for the production of orthoses.

The main advantage of 3D printed orthoses is the correct distribution of pressure along the length of the orthosis and, accordingly, providing the correct pressure for faster recovery from injuries.

Another advantage is the ability to make the orthoses breathable, using various types of structures in their manufacture, while the finished product will not lose its mechanical properties, will be hard, flexible and will hold the limb in the desired position [1].

1.2.   Orthosis definition and classification

An orthosis is a medical product for external use, the main function of which is to restrict the movement of limbs partially or completely in certain directions. It reduces the stress caused by the weight of the limb at the site of injury, speeding healing, reducing pain, and allowing proper movement of the limb.

Orthoses are classified by type of movement, area of application, and specific type of injury. Orthoses are classified by functionality: they can be partially movable or have additional functions. There are static orthoses, which completely limit the movement of joints, ligaments and bones of the limbs, and dynamic orthoses, which have moving parts that allow the limb to function but limit its range of motion. The second type of classification is a classification by area of application, which distinguishes between orthoses of the upper (arm, hand, palm) and lower limb (hips, knees, ankles, feet, legs and combined) and the spinal (neck, chest, spine).

1.3. 3D-printed orthosis production

3D-printed orthosis production is a fast but complex process, and the process of producing orthosis using 3D printing is shown in Fig. 1.1.

Fig. 1.1. 3D-printed orthosis production stages.

The first step is to determine the patient's type of injury and perform appropriate tests. Accordingly, if there are bone fractures or ruptured or sprained ligaments, the injured limb is examined. The second stage is a 3D scan of the limb. Modern capabilities allow the use of a mobile phone with built-in LiDAR and a mobile application, or the use of portable 3D scanners. The next stage is the creation and processing of a 3D model. During processing, a 3D model of the injured limb is created, and redundant information is removed as well as the scanned objects in the background. Next, a 3D model of the limb is prepared for modeling the orthosis. The appropriate size is determined for the model, and the model is cut to leave only the necessary injured part of the limb on which the orthosis will be modeled. The next stage is modeling the orthosis. The necessary parameters are set: thickness, structure, pressure distribution by zone, type of injury fixation depending on the type of injury, and gap between the limb and the orthosis. A modern orthopedic model can be created using artificial intelligence systems. However, the created model must still be checked by a specialist to ensure that there are no errors and that the model has been created correctly. When the model is ready, a manufacturing method is selected. Accordingly, 3D printing uses different methods for manufacturing objects according to the necessary mechanical parameters of the final product, such as flexibility, hardness, etc. If it is possible, the fastest and cheapest method must be selected. Next, the material of manufacture is selected. 3D printing uses various types of thermoplastics, plastic powders, liquid resins, metal powders and carbon fibers (Fig. 1.2).

Fig. 1.2. Materials used for orthosis production using 3D printing.

The next step is to prepare the model for printing. Accordingly, the model support material is used based on the design of the model. The model is cut in layers depending on the required accuracy and layer thickness, balancing between quality and production speed. When the model is ready, it is sent for 3D printing. Once printed, the product is processed and prepared for delivery to the patient. The entire manufacturing process, depending on the technology and parameters of the orthosis, can take from 30 minutes to several hours, but this is the fastest and most convenient process compared to other options, which may also cause discomfort to the user during use [2], [3], [4].

2. 3D PRINTING TECHNOLOGY RESEARCH

2.1. 3D printing definition

3D printing is a method for producing parts and systems that allows for faster production of lighter, stronger parts with complex shapes and designs. In 3D printing, a computer-aided design (CAD) system is used to gradually deposit material, layer by layer, in a certain predefined geometric shape, resulting in a finished part of the volume. The CAD program divides the part into layers of a certain thickness, where each layer creates a path that the printer's print head will follow when placing the material. Each subsequent layer is added to the previous layer of molten or semi-molten material. This type allows the production of complex shaped parts or immediately assembled systems with high precision and without the need for additional processing. AM printing uses thermoplastics, UV resins, metal, ceramics, composite materials, and biochemicals [5], [6].

2.2. Types of 3D printing technologies

3D technologies differ in the type of material used, the type of application of the material, and the type of technology for joining materials. The most commonly used technologies are printing with thermoplastics, thermoplastic powders and UV resins. 3D printing can be divided into seven categories: material extrusion, reservoir polymerization, powder bed fusion, lamination, material and binder jetting, and direct energy deposition categories. The work presents three categories (FDM, SLA, SLS) that can be used for the manufacture of orthoses based on the cost of manufacturing the product, manufacturing speed and availability of technology [3].

Material extrusion technologies use different types of materials that are fed from a printer nozzle. Basically, thermoplastics are supplied from the heated nozzle of the printer, but there are technologies that can also carry out this type of printing with metal, concrete, biological substances and other materials. This category includes FDM, biological printing, construction printing and others. The accuracy of FDM (Fused Deposition Modeling) technology is up to 0.1 mm [7].

The Thesis is devoted to the study of extrusion-type technology (FDM), as a cheap, simple and widespread type of 3D printing technology that can potentially be used in the manufacture of orthoses. FDM is a technology in which the material is fed by a motor to a heated nozzle, where thermoplastics are melted to the melting point of the material and applied layer by layer in accordance with specified settings of the CAD program. The layers are glued together due to the adhesion of the material. Different types of thermoplastics are used: ABS, PLA, PET-G, ASA, PP, PA12, TPU, and others. FDM technology uses thermoplastics that are pre-formed into a solid filament of a specific diameter (usually 1.75 mm or 2.85 mm). FDM printers use a Cartesian or polar coordinate system for three-axis direction: X, Y, and Z (Fig. 2.1) [8].
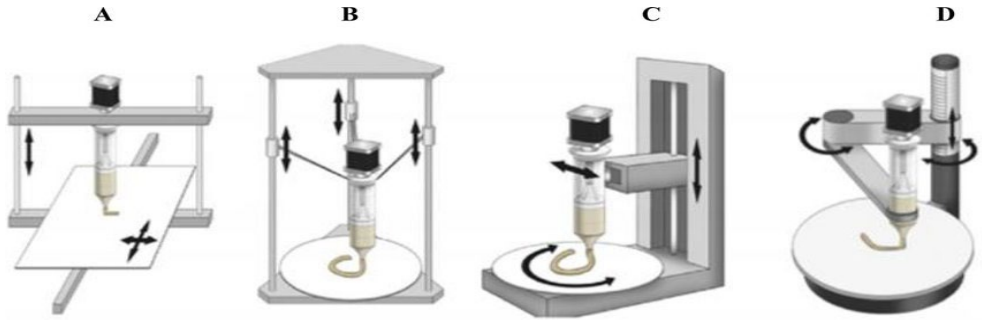
Fig. 2.1. Principle of 3D printing: (A) Cartesian, (B) delta coordinates, (C) polar, and (D) SCARA coordinates [8].

The movements occur at coordinates specified by the CAD software, and the printer feeds the material through a heated nozzle. FDM printers are classified by the type of coordinate system used and the nature of the mechanics (Fig. 2.2). Cartesian rectilinear printers use a three-axis motion to control the position of the printer head, with each axis controlled separately by one or more motors. Cartesian system printers using rectangular mechanics have the following designations: CoreXY, CoreXZ, H-bot, Belt, XZ-Head, and XY-head. Delta printers use three or more rails that connect to the printer head on one side and to the vertical guides on the other side. By adjusting the height of each rail, Z height and X, Y head position can be controlled. SCARA printers use a robotic mechanical arm with a print head attached to the end. Polar printers use a polar coordinate system when printing on a rotating base [9].
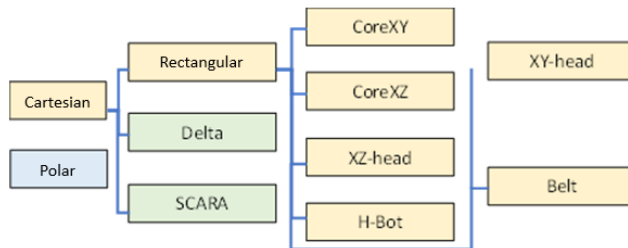

Fig. 2.2. Classification of FDM 3D printers.

FDM technology is taken as the basis to implement the concept and test the theory. The drive and control of FDM 3D printers were investigated. This study investigates FDM technology because most printers in this category can deposit layers in slightly curved paths within the constraints of slope and deposition thickness.

It is assumed that by converting FDM technology to a polar coordinate system, it is possible to print in a Cartesian coordinate system object that cannot be printed by this technology without the use of auxiliary material, which is necessary to reduce printing time and material consumption.

Also, this method will allow you to divide the model into layers from the center of the model to its outer part, thus redistributing the load and reducing the delamination of the model during tension and torsion, which is necessary for the manufacture of orthoses to ensure the necessary rigidity of the structure and to withstand various types of loads.

3. SURVEY OF MODEL PREPARATION METHODS FOR FDM 3D PRINTING

3.1. 3D object position in space and 3D model slicing methods

Although 3D printing holds great promise and is becoming increasingly popular, it currently has many limitations. When it is necessary to produce parts with complex shapes, where there are many hanging elements with a large angle, a support material is usually used. In such cases, additional processing of the model is required. This takes time, increases costs and reduces the surface quality of the manufactured object. To solve the problem, various techniques have been studied, such as changing the shape of the substrates in the support material, using other materials and exploring new materials, and changing printing parameters, but as a result, the problem has not been solved. The problems mainly lie in the orientation of the original object in the environment, its preparation and slicing, since in any 3D printing technology, it is necessary to correctly place the object so that during the slicing stage, there are no elements floating in the air or their printing consists of many hanging elements that are printed at such an angle that the printer cannot print them. The entire printing process is controlled by predefined CAD parameters, so the greatest attention must be paid to the placement of models in the space, model settings adjusting and slicing.

3.2. Study of existing 3D model slicing techniques

Currently, there are a few methods for slicing a 3D model: traditional, multidirectional, and non-layered (Table 3.1). The traditional pattern-slicing method slices the 3D model in equal layers parallel to the platen in a specific linear direction, resulting in a series of parallel layers. The traditional slicing method works well for simple items where there are no hangers or other complex elements.
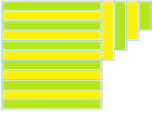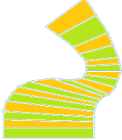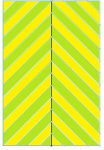
From this method follows the next method – adaptive slicing. In it, the model is still sliced in one direction; however, the thickness of each layer is changed according to the complexity of the object's geometry. The adaptive method gives an opportunity to get better quality when printing objects with not particularly complex geometry, where there are no elements that need to be printed by reorienting the object or changing the slicing direction. Both methods will show layer ladders in the curves of the object surface; as such, slicing methods cannot effectively achieve a flat object surface without increasing the printing time at cost.

If the print object has a complex shape and has many hanging elements, the model can be divided considering the direction of these additional elements, and individual elements can be cut in a more advantageous direction; this type of slicing is called multi-directional slicing. If the object does not have a distinct shape and other slicing methods do not work, the non-layered slicing method is used. Currently, slicing methods are focused on improving the quality of the surface of the printed object and reducing the use of consumables.

The Thesis examines existing methods of slicing objects and proposes its own method, based on a non-layered slicing method, to improve not only the surface quality of printed objects but also to improve the mechanical resistance of objects to various types of loads.

Table 3.1

Existing Methods of Slicing 3D Models

Title	Figure	Description
Traditional method		In the method, the model is cut into parallel layers of equal thickness. The most common and applicable method. Easy to use and universal method. Low accuracy. It is necessary to use a lot of consumables. Overhangs print very poorly.
Adaptive method		Depending on the shape of the object, locally changes the thickness of layers for different elements using contour extrapolation. Increased accuracy in outer perimeters. Good object surface quality. Overhangs print poorly.
Multidirectional method		The object is divided into separate elements and the optimal slicing direction is chosen for each element. It is necessary to use less support material. Difficult to use and requires supervision.
Non-layered method		Automatic detection of overhang elements. Cylindrical coordinate system is used for slicing central axis objects. It is not necessary to use a support material.
Conical method		The layers are cut at an angle, usually in a conical shape. Used to reduce the visibility of layer lines in the final printed object, resulting in a smoother surface finish. Overhangs can be printed without support material.

3.3. Research of the current limitations, challenges and issues of FDM printing

Layered structure of printable objects

One of the most common limitations of FDM printing is the use of a layered structure. The use of layers in 3D printing was proposed as one of the first 3D printing methods, but their use at the same time is a limitation of 3D printing.

A traditional slicing program divides the 3D model into horizontal layers for subsequent printing, and when using the layer structure, visual defects appear as visible horizontal layers on the surface of printed objects. This creates noticeable lines, especially on the vertical surfaces of the object. When printing objects layer by layer, visible layer boundaries are displayed. This effect is also known as the "staircase effect" because of its visual resemblance to the shape of a staircase. Depending on the thickness of the layer, the layering will be more noticeable if the thickness is higher.

Insufficient fusion of layers can lead to poor strength and visibility of boundaries between layers. Improper slicing can create visible layers on curved surfaces that reduce the aesthetics of the printed object.

Layer thickness optimization is used to solve layer structure problems. The selection of the optimal layer thickness is used, depending on the quality and printing time requirements. For example, to create smoother transitions, it is necessary to reduce the thickness of the layer, which requires additional calibration and can increase the printing time. To increase the print quality and further prevent the staircase effect, an adaptive slicing technique is used, which changes the print parameters depending on the geometry of the object, which smoothes the transitions between layers. If the quality of the printed object is unsatisfactory and cannot be corrected by the printer settings, post-processing methods such as sanding are used to further smooth the surface, where additional steps may be required.

When using conical slicing, it changes the slicing angle depending on the geometry of the object, which can smooth the transitions between layers and reduce the visibility of layers on curved surfaces. However, using taper slicing can increase print time and requires careful calibration for optimal results.

In general, a combined approach is used to avoid the visibility of the interlayer transition. Solving the problem requires an integrated approach, which includes both the improvement of slicing algorithms and the development of new technologies and equipment. It is important to continue research in this area to improve 3D printing technology. Development of more efficient non-planar slicing algorithms is needed, considering printing speed and surface quality. The application of neural network methods is required so that the neural networks can optimally select the slicing parameters for each object. Non-planar slicing methods provide promising solutions for improving the quality of 3D printing by reducing the visibility of layers and creating smoother surfaces [10].

Use of overhangs and support material

Overhangs are parts of an object that protrude into the air without direct support from the previous layer. During 3D printing, there are cases when, due to the complex structure of a printable object, part of the elements are printed in the air at a certain angle. Several slicing methods use a backing material to stabilize the protrusions during the printing process and for the overhang to print on the backing material. Overhang angles that are too steep can cause difficulties with support and stabilization. Overhangs can be classified by the inclusion of elements in the contour and by the type of use of supports. In the classification by contour, it is divided according to the fact that the contour elements of the next layer are included in the contour of the previous layer and four types are defined as shown in Fig. 3.1[11].
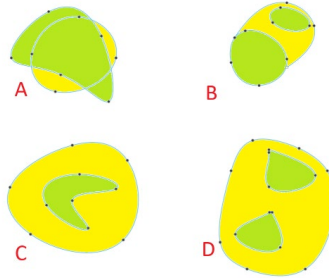
Fig. 3.1. Classification of overhang elements by contour type: A – fragment; B – complex fragment; C – single contour or ring; D – complex ring [12].

According to the type of use of supports, three types of overhang are distinguished, shown in Fig. 3.2 downward extension, micro-overhang and macro-overhang [13]. A micro overhang is an element where the outer perimeter of the previous layer is larger than the previous layer. This type of overhang can be printed without a support material, depending on the angle of inclination and the properties of the material. Macro overhangs are overhangs that can be printed without support material. If the overhang is connected to another element to be printed, and if there is no such element, then it is necessary to use supports. A descending extension is a type of overhang where the element is not connected to the base object and cannot be printed without the use of supports [14].
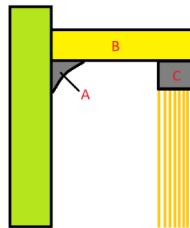

Fig. 3.2. Types of overhang: A – micro-overhang; B – macro-overhang; C – downward extension [13].

Support material is used to support the protruding parts of the object during printing, preventing collapse due to gravity. Current moment slicing CAD programs include functionality to automatically create supports based on object geometry. However, support marks can leave visible marks on the print surface that require additional processing to remove them after printing. It also uses printable model placement optimization to reduce overhang angles, which can reduce the need for supports; however, this limits the appearance of the printable object and cannot be applied to complex object shapes [15].

Various random slicing methods are used to solve the problem, such as the conical slicing method. The basis of the conical method approach is to change the angle of inclination of the overhang elements, forming a conical shape. This method improves overhang support and stability, reducing the risk of collapse and reducing the need for support. It reduces the steepness of the overhang angle, which reduces the possibility of flattening during the printing process. The conical shape of the layers creates a wider contact surface with the previous layer,

which provides better support during printing. This method can be adapted to different geometric shapes, making it a universal solution for different objects. However, the taper method may have limitations when applied to too steep overhang angles and must be carefully tuned for optimal results, which may require time and experience, and more work is needed to optimize and calibrate this method.

The angle of application of the material and the distance of the print head from the printing table

After researching the overhang problem and proposing a solution to use conical slicing, a problem arises related to the printing of overhang elements with the nozzles of an existing 3D printer. Existing 3D printer nozzles have a conical 45° angle shape and are usually placed directly perpendicular to the printing table due to the physical limitation of overhang printing angles. Cartesian FDM 3D printers can print overhangs with an overhang angle of up to 45° (Fig. 3.3).
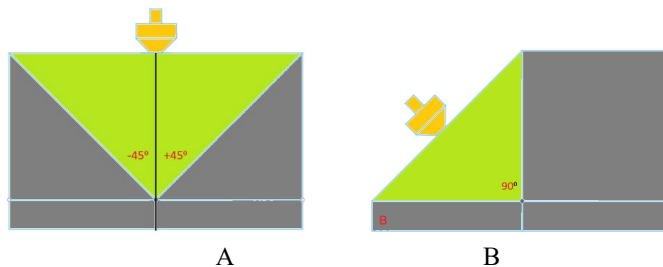

Fig. 3.3. The overhang angle depends on the position of the print nozzle:
A – perpendicular to the printing table, B – with an offset of 45°.

This limitation results from the design and position of the nozzle, as well as from the way the material is applied. This limitation strictly determines in what way and how complexly shaped objects can be printed. Accordingly, the application of the conical method of printing is limited by the design of the 3D printer, and the existing position of the nozzle does not allow the effective use of this method because there is a problem related to the feeding of the material, or an extrusion problem when the nozzle starts to touch the already extruded material at steep angles (Fig. 3.4).

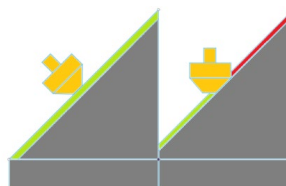Fig. 3.4. The problem of conical print extrusion [16].

One of the ways to increase this angle is to turn the nozzle to an angle of 45°; in this way, it is possible to print overhangs up to 90°. Such a solution has been used in timing belt 3D printers; however, the conical method cannot be used for such printers due to the design of the printer, as their print head movements are limited by the extrusion problem [17].

LITERATURE REVIEW SUMMARY

At the current moment, the problem with the use of support material and overhangs in 3D printing is still relevant, especially when creating complex geometric shapes and overhangs. The use of layer-slicing techniques still affects the aesthetics and mechanical strength of printed objects, especially in FDM printing. The use of adaptive slicing methods, new types of supports and optimized slicing algorithms can reduce the visibility of layers and improve the overall print quality but do not completely solve the problems; accordingly, it is necessary to use new combined methods, such as multi-directional slicing and non-layered slicing methods, to provide more comprehensive and efficient solutions. A key factor in the development of new problem-solving methods and techniques is systematic testing and experimentation, and further optimization of 3D printing and calibration parameters is required to achieve the best results. Conical or cylindrical non-layered slicing methods create great potential and offer more possibilities, and within the framework of this work, solutions based on the basics of these methods will be used and proposed. Overall, FDM printers provide the ability to produce orthoses that are adjusted to the patient's anatomy and can meet the basic requirements of medical orthoses.

FDM technology is a relatively affordable and cost-effective 3D printing method that can be attractive from an orthotic manufacturing perspective, as FDM 3D printers are easy to use and have a simple design that facilitates maintenance and staff training. However, due to the layered structure, the existing traditional type of 3D printers cannot offer competitive mechanical parameters compared to other fabrication methods and technologies, and the use of non-layered slicing can provide a competitive solution as well as efficient and cheap manufacturing, which can radically change the situation of the market and the use of 3D printing technology in the field of medicine.

After researching the existing limitations of FDM Cartesian 3D printing, their solutions and existing 3D model slicing methods, it was found that the most promising printing method is non-layered printing, but currently, there is no convenient and unified solution and software for its implementation. It was decided to create a methodology through which non-layered printing can be achieved using available open access and common traditional pattern preparation methods while providing a technical solution for switching printing methods to expand the possibilities of existing solutions on the market.

As part of the Thesis, it was decided to develop a 3-axis cylindrical non-layered printing method using existing traditional model preparation solutions, build a 3D printer prototype to confirm the concept, and conduct testing and experiments to compare with traditional and adaptive slicing methods, which are currently more common and cheaper solutions. The second stage is to develop a multi-axis non-layered slicing method based on the results of the 3-axis method and the prototype, build a prototype, and compare the two new methods, the complexity of their use, and efficiency and adaptability for orthosis manufacturing, as well as draw conclusions about the work done and offer recommendations for future improvements.

EXPERIMENTAL PART

4. RESEARCH AND DEVELOPMENT OF A NON-LAYERED SLICING METHOD FOR MANUFACTURING ORTHOSIS, PROTOTYPE DEVELOPMENT AND METHOD ADJUSTMENT

4.1. Cylindrical 3D printing method development

Based on the collected literature, it has been found that orthopedic products usually have a variety of complex shapes and curvatures and can be cylindrical or semi-convex, which means that their cylindrical nature must be taken into account for their 3D printing. The method to be developed is intended to improve the printing quality of cylindrical products. One way to achieve this is to use a flat printing surface and round it so that the edges of the plane meet to form a cylinder. This surface will be closed, providing unlimited table length. In traditional layer-by-layer printing, transferring to a cylindrical surface will produce cylindrical objects. This transformation of surface is shown in Fig. 4.1.
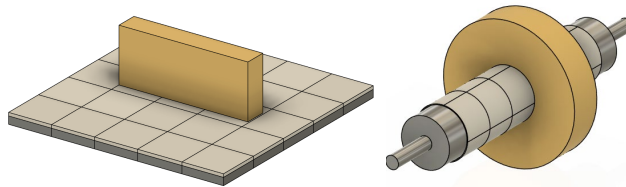

Fig. 4.1. Transition from flat layer printing to cylindrical printing.

In traditional methods, you can change the fill angle of a layer in a single layer, and if you use this approach in cylinder printing while changing the fill angle perpendicular to the angle of the previous layer, the layers form a dense network of lines. The applied material, then, in this way, the most optimal printing of curved or cylindrical products can be ensured without using supports. Printing of similar products on a flat surface will be done layer by layer, so the layers will be held together only by the adhesion of the material, and additionally, supports will have to be used, as it will not be possible to position the object for printing without using supports (Fig. 4.2).
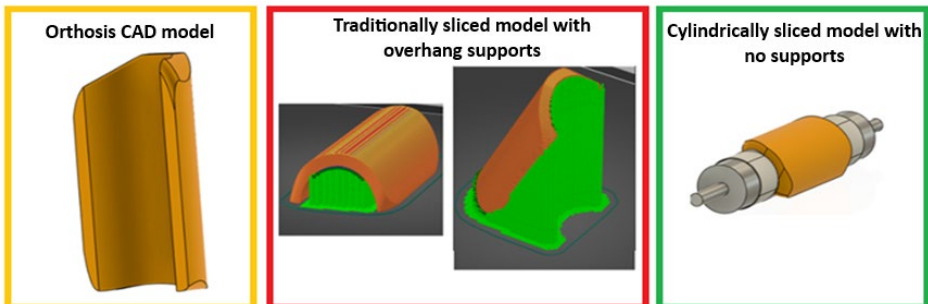

Fig. 4.2. Placement of a cylindrical object in traditional and cylindrical methods.

4.2. Calculations of experimental bench parameters

Based on how the placement of cylindrical orthoses is optimal using a cylindrical printing table, it was decided to develop an experimental stand for the approval of printing methods. It is intended to create a rotary printing cylindrical table connected to a stepper motor and controlled by a control board based on a microcontroller. A print head with a 0.4 mm nozzle, which uses a 1.75 mm thick filament with a line thickness of 0.4 mm, is adopted as the experimental bench to be developed. In order to achieve the accuracy required for the successful application of the material to the cylinder, it is necessary to calculate the minimum angular accuracy to which the rotor of the stepper will turn for one step of the stepper motor. The angular accuracy, Θ, can be calculated according to Formula (4.1) [18]:

$$\Theta = \frac{nozzle\ accuracy}{maximum\ print\ radius} = \frac{0.4}{10} \times \frac{180}{\pi} = 2.29^0 \tag{4.1}$$

It is assumed that the angle of one step of the stepper motor is 1.8°, which corresponds to the more common angle of NEMA 17 stepper motors [19], then the necessary ratio R (4.2) of the transmission mechanism between the stepper motor and the cylindrical printing table can be calculated:

$$R = \frac{motor\ pitch\ length}{angular\ accuracy} = \frac{1.8}{2.29} = 0.78 \tag{4.2}$$

To calculate the torque of the stepper motor, it is necessary to determine the mass moment of inertia Ig and the minimum angular acceleration α. The mass moment of inertia I_g of the stand can be calculated by defining the total mass moment of inertia of all components, which is calculated using Formula (4.3).

$$I_g = \frac{1}{2}\rho\pi L r^4 = \frac{1}{2}Mr^2, \tag{4.3}$$

where
 r – the radius of the printable object, m;
 L – the length of the printable object, m;
 ρ – the density of the printing material, kg/m^3;
 M – the mass of the printable object, kg.

The total moment of inertia of the calculated bench elements is equal to $I_g = 0.00474$ kg/m^2.

Angular acceleration is the rate of change of angular velocity with time (4.4), and if we assume that the average rotation speed of the cylinder is 500 rpm and the change of velocity takes place in 1 second, then the calculated angular acceleration is about 50 rad/s^2.

$$\alpha = \frac{\Delta\omega}{\Delta t}, \tag{4.4}$$

where α is the angular acceleration, rad/s^2; $\Delta\omega$ is the rotation speed, rpm; and Δt is time, s.

The torque of an experimental bench is calculated as the product of mass moment of inertia I_g and minimum angular acceleration α (4.5):

$$M = I_g \times \alpha = 0.00474 \times 10 = 0.0474\ Nm \tag{4.5}$$

4.3. Development of an experimental cylindrical 3D printing bench

A cylindrical printing test bench has been created for the approval of the following concepts. The components of the stand are listed in Table 4.2.

Cylindrical 3D Printer Stand Components

Title	Model	Parameters
3D printer frame	Creality Ender-3 V2	CoreXZ Cartesian FDM 3D printer
Stepper motor	1 × NEMA 17 42-34 BJ42D15-26V12	Pitch angle: 1.8º, rated current 0.8 A, number of phases: 2, torque: 0.8 Nm
Stepper motor driver	Pololu RepRap A4988	Operating voltage: 8–35 V DC, logic voltage: 3–5.5 V, Imax 2A
Power supply	Meanwell LRS-350-24	24V DC, 350W, 14.6 A, 48-63 Hz
Control microcontroller board	Arduino Nano	ATmega328P CH340 microcontroller, 14 digital outputs, 6 PWM outputs, 8 analog outputs, operating voltage 5 V, logic voltage 3.3 V
Transmission mechanism	Two 20 tooth GT2 gears, 124-2GT-6 belt, 2 × 688ZZ bearings, 100 mm × 8 mm rod	1:1 gear ratio
Software	Arduino IDE	Open source firmware for the RepRap family of 3D printers

The stand is based on the components of a classic RepRap 3D printer, and its task is to control the possibility of printing on a rotating cylinder by replacing the Y-axis from moving the flat table to the rotating cylinder. The prototype is built on the basis of the Creality Ender-3 V2 printer [20], taken as a classic representative of FDM printers, where the 3D printer has a switched Y-stepper motor responsible for moving the printing table in the Y-plane. A 3D printed and assembled test bench is placed on the printing flat table, which is fixed and remains in one position, which combines a gear mechanism and a stepper motor with a gear ratio of 1:1 using two 2GT 20 teeth gears. Such a ratio corresponds to the minimum necessary ratio to achieve printing accuracy. The test bench is positioned so that the axis of the rod coincides with the direction of the X-axis and the two axes are parallel. The test bench and its location are shown in Fig. 4.3.
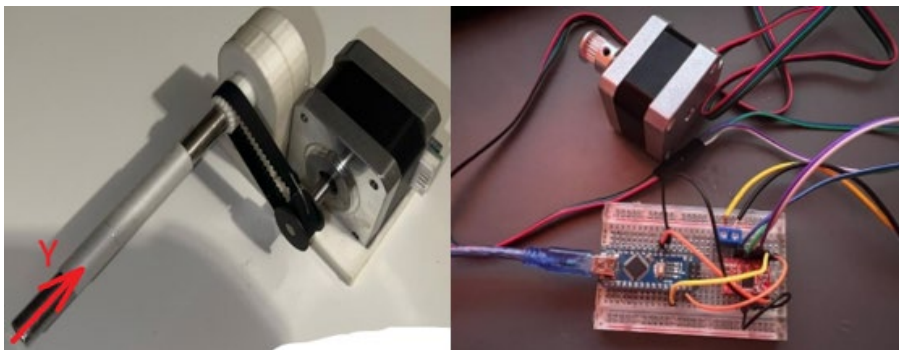

Fig. 4.3. Experimental bench and its control elements.

The Y-axis control of the rotating cylinder is provided by the BJ42D15-26V12 stepper motor and the A4988 stepper motor driver controlled by the Arduino Nano control board, and the axis movement is controlled by the code written in the Arduino IDE environment. The movements of the Y-axis are synchronized with the control code of the 3D printer by manually changing the slicing speed of the Y-axis and the number of steps per millimeter ratio. The connection of the elements of the test stand is shown in Fig. 4.4.
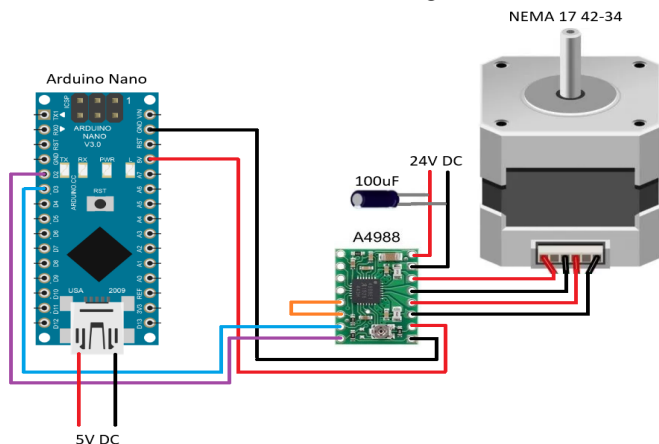

Fig. 4.4. Circuit of the cylindrical printing test bench elements.

The Arduino Nano control board is powered by USB 5 V DC. Stepper motor driver control is realized by connecting to Arduino 2 and 3 digital output and to 5 V DC and GND output. The driver is powered by a Mean Well 24 V DC switching power supply, with an additional 100 µF capacitor connected to reduce voltage spikes. The block, in turn, is connected to a 230 V 50 Hz AC network. The stepper motor winding is connected to the output of the stepper motor drivers 2B, 2A and 1A, 1B. The SLEEP and RESET outputs of the A4988 driver are connected separately to supply the HIGH signal to the SLEEP output, which is necessary for the driver to operate. The stepper motor is housed in a transmission mechanism and is connected to a steel 8 mm diameter rod using 2GT 20 tooth gears and a 2GT 100 mm timing belt.

4.4. Conducted experiments and summary of results

Different types of flat-shaped CAD models (Fig. 4.5) have been prepared for test printing, cut with the traditional slicing method in the Prusa Slicer program, printing material PLA, printing temperature 230 °C [21]. The result is objects of cylindrical shape (Fig. 4.6).
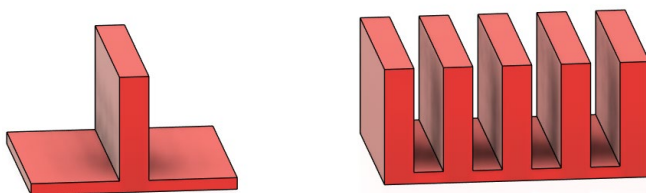

Fig. 4.5. CAD models prepared for test printing in the Autodesk Fusion 360 program.
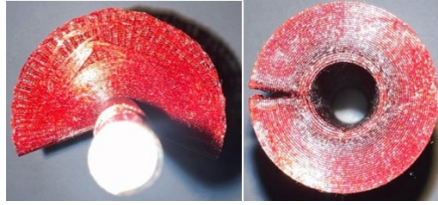
Fig. 4.6. Cylindrical printing results and proof of defects.

In the obtained samples, without pre-processing, the geometry of the models is deformed, and if the initial printed layers connect with the edges to form a whole cylinder, then as the number of layers increases and the diameter increases, the edges of the object begin to move away, forming a gap.

To check the possibility of changing the filling angle of the layer and the perpendicular overlap of the layers, a CAD model of a cylinder with a diameter of 8 mm and a length of 50 mm with a layer thickness of 1 mm was prepared. In version B, the cylinders were cut with the traditional printing method, where the layers run parallel to each other; in version A, plane models are prepared, where each subsequent layer has a filling that goes perpendicular to the angle that was in the filling of the previous layer. Plane models were printed on a cylindrical platform and the result were cylinders with the required parameters. The result is shown in Fig. 4.7.
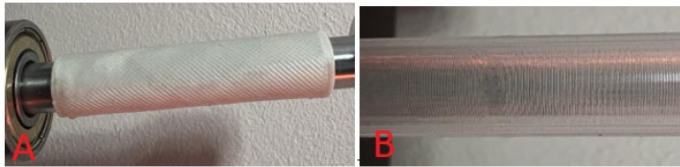

Fig. 4.7. Test bench print results for material coating test on cylinder examples: B – a conventional method example, and A – an example of a cylindrical method.

You can see that the layers of the first variant are placed parallel to each other, while in the second variant, they cross to form the shape of the mesh filling. All models are prepared with 0.3 mm layer thickness, 0.4 mm line thickness, 60 mm/s print speed and 500 mm/s^2 accelerations. Creality PLA white sharp and Creality PET-G transparent filaments are used as printing material. The printing temperature is 230 °C, the printing speed is 60 mm/s, and the accelerations are 500 mm/s^2.

4.5. Conclusions of the proof of concept

The transition to the cylindrical coordinate system is that the length of the arc in one layer of the object is constant when the length of the arc of the cylinder increases all the time, and the absence of a missing arc is reflected on the printable object. So, it is necessary to additionally process the model during the model preparation stage to eliminate this defect. It has also been confirmed that as the amount of layers increases and the height of the model increases, a lack of material extrusion occurs, which manifests itself as a lower density of the model and noticeable printing imperfections. As a result, it is necessary to develop a 3D printing method that could eliminate the identified shortcomings.

5. THREE-AXIS FDM CYLINDRICAL 3D PRINTING METHOD AND PROTOTYPE DEVELOPMENT

5.1. Development of a cylindrical slicing method for FDM 3D printing

Based on the results of an experimental bench, a full-fledged cylindrical FDM 3D printing method has been developed. In the manufacture of orthotics and other orthopedic products, where the products are designed to be worn on the body and subject to various types of loads, there are several limitations related to the mechanical properties and durability of the finished products. Existing traditional 3D slicing methods used in current slicing programs rely on a layering strategy where each layer is printed horizontally, creating an inter-layer connection, which is a potentially weak point of the product. These inter-layer joints are less resistant to tension in the direction perpendicular to the layers, which can cause the product to delaminate and fail if an appropriate load is applied. This is especially important for orthoses that must withstand various types of mechanical stress during use. Products made with the traditional 3D printing method have limited resistance to torsional loads acting in the plane of the layers. This is because the internal structure of the product is formed by consistently applying layers, which create the conditions for the generation of stresses when the material intertwines. As a result, the application of such loads can lead to deformation or collapse of the product along the layers, which reduces its functionality and reliability. In addition, suboptimal support and print path distribution can lead to inefficient use of material and an increase in printing time. At the same time, horizontal slicing limits design options, especially when complex anatomical shapes must be accurately reproduced [22], [23], [24].

The cylindrical slicing method developed in the Thesis offers a solution to these problems by changing the orientation and strategy of the layers of the product structure. With cylindrical slicing, the layers can be oriented to better distribute the load, including perpendicular to the direction of the layers, which increases the overall tensile strength of the product. By optimizing the structure of the layer in the direction of loads and in the transverse direction, the products become more resistant to the effects of torsion, which is especially important for orthoses exposed to complex dynamic loads during operation. The cylindrical slicing method not only improves the mechanical properties of the products due to more efficient load distribution but also expands the design possibilities, allowing the creation of more complex and reliable structures.

An applicable method combines geometric optimization with variable layer fill angle to reduce tensile stresses using a standard layer slicing method but printing on a rotating cylinder. The use of a cylindrical shape for 3D printed objects improves the mechanical properties of the printed products, increasing their resistance to tensile loads and delamination. The layers of the cylindrically shaped product are pressed against each other, creating a physical constraint, effectively preventing delamination, a common problem in standard multi-layer constructions (Fig. 5.1).
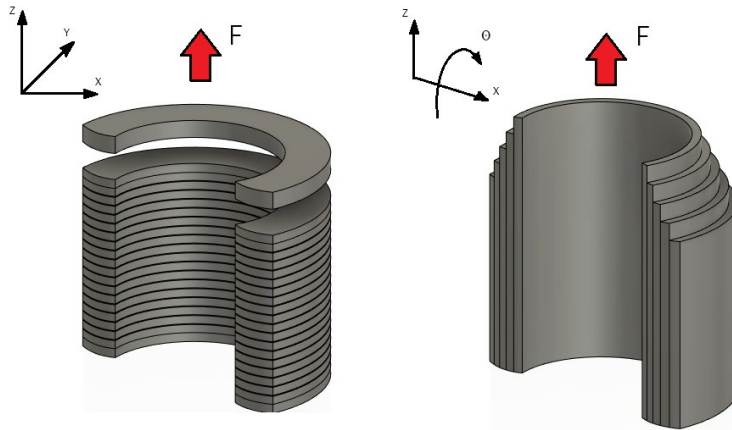
Fig. 5.1. Arrangement of layers in Cartesian and cylindrical coordinate system.

It is assumed that the layers are placed so that 100 % of the material of the layer is in contact with 100 % of the material of the other layer and there is no gap between the layers, then the adhesion of the layers is based on the parameters of the printing material, or adhesion and the contact area of the layers. However, usually, the layer material is not applied 100 % perfectly, and as a result, there are gaps between the layers. This parameter is defined by the parameters of the object to be printed and the 3D printer used, and it can only be directly influenced by changing the printing parameters (layer thickness, extrusion parameters, printing speed).

There are two options for increasing the adhesion of the layers: changing the material parameters and increasing the area of connection of the layers. In the Cartesian system, the layers are placed parallel, and you can directly increase the connection area of the layers by changing the filling percentage of the printable object; however, if the filling is already 100 %, then it is no longer possible to increase the connection areas. However, when moving to the cylindrical coordinate system, due to the cylindrical shape, the joint area of the layers increases, as well as the layers begin to stick to each other due to the cylindrical arrangement, where the layers are interconnected, and the load vector changes (Fig. 5.2).

The length of the connection of the layers in the Cartesian system,

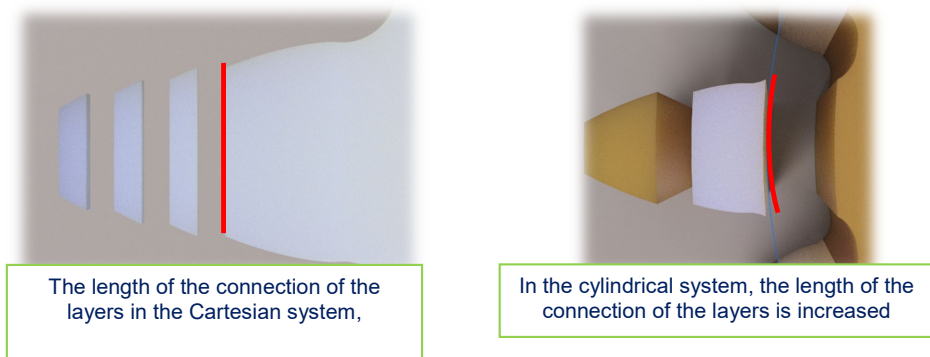In the cylindrical system, the length of the connection of the layers is increased

Fig. 5.2. Increased interlayer bonding area.

The idea of the method to be developed is to replace the Y-axis with a rotating cylinder using a Cartesian coordinate system 3D printer in such a way that minimally changing the configuration of the 3D printer leads to the cylindrical coordinate system. The main problem that arises when using the cylindrical system is the absence of software for preparing CAD models; all existing solutions offer simple traditional or adaptive slicing, which does not allow the full use of the given method. That is why it was decided to develop an approach that will allow the use of this type of printer more freely and understandably. One of the approaches used in previous studies is to cut the existing CAD model in a freely chosen place and straighten it in a flat way (Fig. 5.3) [25].
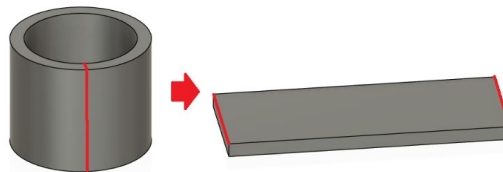

Fig. 5.3. Slicing and transforming a cylinder into a plane.

Two CAD model straightening techniques are used in the Thesis: straight flat straightening and spiral straightening. In the straight flat straightening cylindrical object is cut at a freely chosen location along one axis. When a straight, straightened object is printed, the two edges of the object along which the pattern was cut are joining together and create a visible seam. Straight straightening is worth using when the effect of the seam does not affect the use of the object to be printed or when you need to print a non-enclosed cylindrical object whose edges are not connected and which has an arc shape (Fig. 5.4).
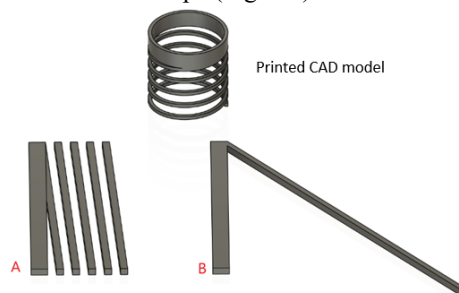

Fig. 5.4. Straight planar (A) and helical (B) straightening of the CAD model.

For complex geometric shapes and models with several layers with a relatively high height, this type of straightening will distort the original geometry since the rotating printing cylinder (printing table) has a certain diameter, and this parameter will be different for each layer, depending on the layer thickness. Therefore, it is necessary to use complex straightening algorithms, which already calculate the thickness of the layers before slicing the model (Fig. 5.5). The second problem is that when preparing models for printing with Cartesian-type traditional slicing programs, the program will calculate the specified amount of material for each layer, but depending on the thickness of the layers, the amount of material for each layer will increase; and as the number of layers of the resulting object to be printed increases, the amount of supplied material will decrease to the specified percentage (Fig. 5.6). As well as

within one layer, due to the difference in the length of the inner and outer cylinder line, the material will be distributed unevenly (Fig. 5.7); however, this drawback can be minimized by changing the height of the layer nozzle.
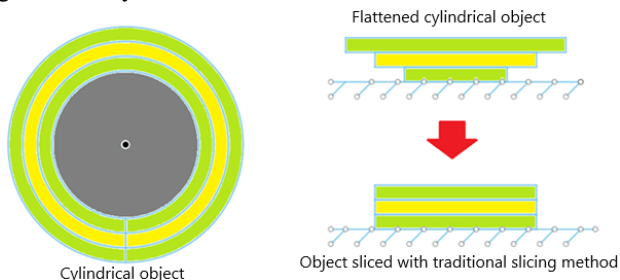
Fig. 5.5. Deformation of the model during the straightening process.
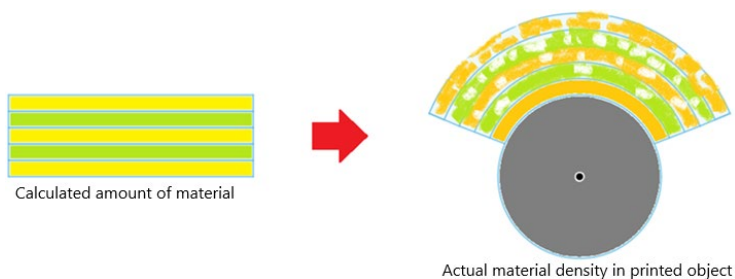
Fig. 5.6. Insufficient amount of fed material problem.
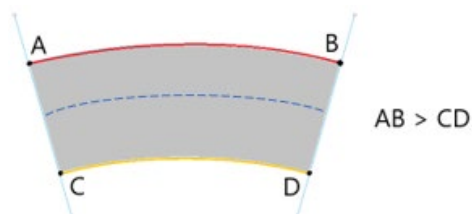
Fig. 5.7. Distribution of material within one layer.

The method to be developed in the Thesis is adapted to the manufacture of orthoses. When the parameters of the orthosis are defined (see Chapter 1) and if the geometry of the straightened orthosis is close to a completely flat shape, it is possible to prepare the initial CAD model as a flat object. The second task is to eliminate the problems inherent in the cylindrical slicing method. Based on these parameters, a new method of preparing models was created. A schematic print preparation process is shown in Fig. 5.8.
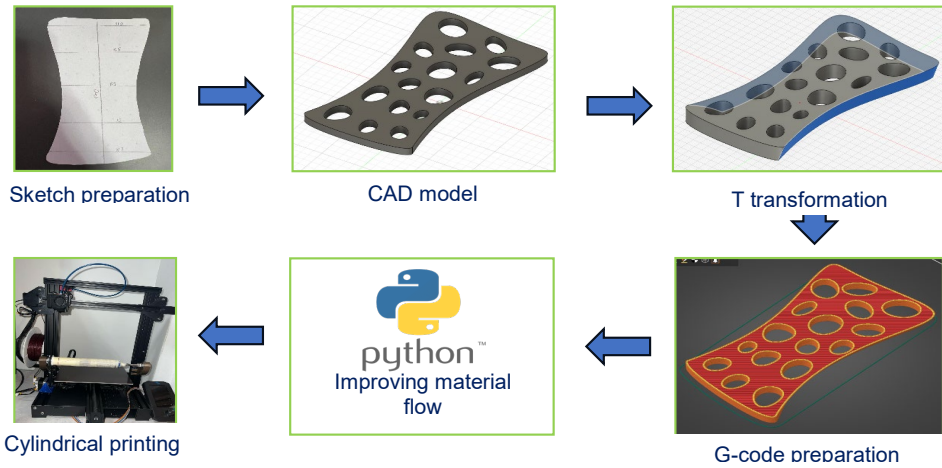
Fig. 5.8. Strategy of a new cylindrical model preparation method.

In the first step, the parameters and dimensions of the human limb are taken, and a simple physical flat orthosis model is created, which is transferred to the CAD program as a CAD model. Based on the sketch, a CAD 3D model of the orthosis is created in a simple Cartesian coordinate system in CAD software and is saved in STL or OBJ format. In this work, Autodesk Fusion 360 is used, but it may be any free open-access software. Flat model edges must be perpendicular to the flat printing surface to avoid geometry deformation during the rounded printing process.

The next step is to apply a new T transformation to the flat CAD model. The purpose of this transformation is to prepare the model for cylindrical printing by changing the geometry of the object edges to make a fully enclosed seam for enclosed models or to make perpendicular to rotating cylinder (printing surface) edges for non-enclosed models. This transformation is needed to eliminate flat slicing geometrical issues when printing on round surfaces as angle φ that occurs because of layer elongation during object rounding.

In rounded printing, each next layer is a little bit longer than the previous layer, and it is needed to calculate how long a distance each layer increases and how much material needs to be provided during the extrusion processɪɔ T-transform was developed as a Python code that reads 3D model files in STL or OBJ format. This code requires input of the initial parameters of the model, such as the height of the print layer, the axis to be used for edge deformation, and the diameter of the rotating cylinder to calculate the distance to be deformed.. After code compilation, a new CAD model is generated to be used in FDM Cartesian slicing software, where the model is sliced according to defined layer height and material parameters. PrusaSlicer 2.8.0 slicing program was used.

After the traditional slicing process G-code of the modified flat 3D model is obtained, and the next step is to adjust the extruded material amount according to non-planar printing needs. For these purposes, we developed another Python code that reads generated by slicer G-code, then we must input printing cylinder diameter to calculate the extrusion magnification factor (Equation (5.1)). Python code (Appendix 3) will read the layer height, then calculate each layer

arc length, and according to new parameters, it will recalculate the extrusion amount for each layer and rewrite the G-code extrusion commands.

$$magnification\ factor = \frac{thickness\ of\ an\ existing\ layer \times 2\pi}{layer\ arc\ length} \qquad (5.1)$$

This code calculates the required amount of material by reading the prepared G-code and substituting the indicated amount of extrusion for the required amount of extrusion for quality printing. Once the final G-code is obtained, it is sent to be printed on a cylindrical type of 3D printer, and the printed result is an orthosis with increased mechanical strength, printed without support material and eliminating overhang printing problems.

As a result, the G-code of the modified flat 3D model is obtained with adjusted extrusion commands. This G-code is sent to a reassembled FDM 3D printer with one changed axis to a rotating cylinder mechanism. To ensure different model sizes, printing cylinders must be easily changeable. To ensure better adhesion between the printing cylinder and the printed object, the cylinder must be heated or coated with adhesion materials.

To approve the concept of the provided method, the 3D concept of a cylindrical 3D printer was modeled, and then based on the modeled concept, the FDM Creality Ender 3V2 3D printer was used, that has been modified. The Y-axis, which ensures horizontal print head and rail movements in the Y-direction, was modified to a rotating cylinder that is controlled by the NEMA 17 42-34 stepper motor. To ensure all needed stepper motor and sensors connections and control abilities, the Wi-Fi control printer motherboard was changed to Bigtreetech Manta M8P board with STM32H723ZET6 microcontroller and installed Raspberry Pi CB4 board. For stepper motor control,TMC2209 stepper motor drivers were used. Rotating cylinder assembly and connection parts were 3D printed of Fiberlogy nylon PA12 material.

Description of the CAD model preparation method and the performed calculations

The T transformation is designed to compensate for the angle that occurs when switching from the Cartesian system to the cylindrical coordinate system, where the ratio of the height of the layer to the line length of the cylinder occurs. Wrapping the flat pattern around the cylinder causes the vertical edges of the pattern to curve and, therefore, changes the angle they make with the base. The print cylinder has a curve, and when a planar pattern wraps around that curve, the inner and outer edges of the pattern curve differently. The bottom edges of the model are closer to the center of the cylinder and, therefore, have less curvature compared to the top edges. To compensate for this effect and also to make the upper ends of the model blend together, the model must first be assembled. This curvature should correspond to the curvature of the cylinder so that after wrapping the model around the cylinder, all edges remain perpendicular to the base of the cylinder (Fig. 5.9).
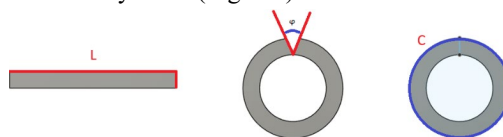

Fig. 5.9. The T transformation of models applicable for minimizing the angle φ on the model to create a non-visible seam.

It is needed to:

1) measure the radius of the printing cylinder R (mm);
2) calculate the arc length C (mm), which will be formed by the upper edge of the model after wrapping around the cylinder;
3) based on the arc radius R and length C, calculate the angle of curvature change φ for the upper side so that it remains perpendicular to the base after wrapping.

The transformation can be expressed by Formula (5.2), where π is equal to 3.1415:

$$C = 2\pi R, \qquad (5.2)$$

where C is the length of the cylinder rim, mm, and R is the radius of the cylinder, mm.

If the length of the model is equal to L, then the angle φ can be calculated as (5.3):

$$\varphi = \frac{L}{C}, \qquad (5.3)$$

where φ is the offset angle, °, L is the length of the edge of the model, mm, and C is the length of the cylinder rim, mm.

With this calculation, the offset angle φ, to which it is necessary to transform the model, can be determined. However, due to the fact that the change to the cylindrical coordinate system occurs with only one axis change, it is also necessary to change the model only in the Y direction without changing the X and Z coordinates. To realize this, a Python code has been written that reads the STL model, determines its coordinates and shifts the coordinates of the Y-axis direction of the model to the specified distance, which is calculated from the geometry parameters of the model.

In the Thesis, it is assumed that the diameter of the printing cylinder is 32 mm; then if we assume that the thickness of the layer is 0.3 mm, the parameters for the model with five layers are summarized in Table 5.1.

Table 5.1

Calculation of Arc Length and Offset Angle of Cylindrical Samples

Layer number	Layer thickness, mm	Diameter, mm	Arc length, mm	Offset angle, °
0	0	32	100.48	0
1	0.3	32.6	102.364	0.586144
2	0.6	33.2	104.248	1.151101
3	0.9	33.8	106.132	1.69600
4	1.2	34.4	108.016	2.221893
5	1.5	35.0	109.900	2.728952

A method of improving the amount of material feed

The second thing, how the amount of material feeding changes, is related to the fact that in a cylindrical coordinate system when moving from one layer to the next, it is necessary to increase the amount of material fed because as the height of the layer increases, the distance of the print nozzle from the center of the print cylinder changes, as the diameter increases. As the diameter of the object to be printed increases, so does its length. When calculating the percentage change in arc length from layer to layer, we see that the increase in arc length of the

next layer remains relatively constant (because each layer adds the same thickness), but the base of the percentage calculation (i.e. the arc length itself) increases. When adding the same layer thickness to a larger diameter, the increase in arc length remains similar, but relative to the total arc length, the increase is a smaller and smaller percentage (Table 4.5). This is because the percentage change is calculated as the ratio of the increase to the original value. As the initial value (arc length) increases with each layer, the same absolute increase represents a smaller fraction of this increasing initial value. If you add the same amount of material to layers of different diameters, that amount will make up a smaller percentage of the total size of the larger layer compared to the smaller one.

While the amount of material added (and therefore the increase in arc length) may be constant, the percentage of this increase in total arc length decreases as the diameter of the object increases. Accordingly, there are two options for calculating the volume of material supply.

•   The first option is to calculate the total percentage increase for each layer based on the dimensions of the original print cylinder, such that the percentage increase will be calculated from the total percentage increase, and the percentage increase will decrease linearly with the height of the layers. Accordingly, it is necessary to more accurately calculate the increase percentage when paring to each next layer, which is not optimal when processing large-volume codes.

•   The second option is to calculate the material increase percentage of the next layer based on the arc length of the previous layer.

If it is assumed that the thickness of the layer is constant and the model is cut using the traditional method, then in both variants, the actual increase percentage will remain unchanged; however, as the height of the layer increases in the first option, it is necessary to re-transfer the increase percentage, or use the complex formula to calculate the amount of material.

In the second option, knowing the thickness of the layer and the diameter of the printing cylinder, you can initially calculate the percentage of increase from layer to layer and apply that percentage of increase to the next layer; in this way, there is no need to perform complex calculations for calculating the amount of extrusion.

Both variants are used and compared in the Thesis; however, in the cylindrical prototype variant, a dynamically calculated coefficient is used, which dynamically calculates the extrusion coefficient and provides a faster and more efficient extrusion calculation (Fig. 5.10).
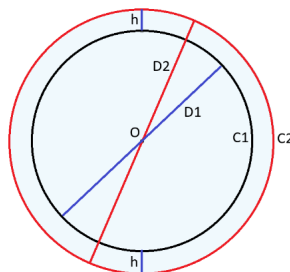

Fig. 5.10. Layer arc length calculation.

Initially, it is necessary to calculate the arc length of the printing cylinder (5.4):

$$C = \pi D, \tag{5.4}$$

where C is the arc length, mm, and D is the diameter of the cylinder, mm.

When we add layer height h to the cylinder, the diameter increases by $2h$ because the addition is on both sides of the cylinder, which affects the length of the arc. The percentage change in extrusion can be calculated by comparing the arc length before and after adding the layer. If the initial length of the arc is C_0, and the length of the arc after adding the layer is C_1, then the percentage change can be expressed in P as in (5.5):

$$P = \left(\frac{C_1 - C_0}{C_0}\right) \times 100\ \% \tag{5.5}$$

If initially, the diameter of the cylinder is D_0, then after adding the first layer, the diameter will become $D_0 + 2h$ and the length of the arc will change accordingly. Assuming that the extrusion changes proportionally to the arc length, the percentage change in extrusion after each new layer corresponds to the percentage change in the arc length.

Calculation example where the diameter of the printing cylinder is equal to 30 mm and the thickness of the layer is defined and is 0.3 mm in each layer is as follows:

1. The arc length of the print cylinder is $C_0 = \pi \times 30 = 94.25$ mm.
2. The diameter after adding layer $D_1 = 30 + 2 \times 0.3 = 30.6$ mm.
3. The arc length of the new layer $C_1 = \pi \times D_1 = 96.13$ mm.
4. The calculated percentage of material increase $P = \left(\frac{C_1 - C_0}{C_0}\right) \times 100\ \% = 2.00\ \%$

The initial arc length is approximately 94.25 mm. After adding the first layer with a thickness of 0.3 mm, the new arc length is approximately 96.13 mm. This means that the percentage change in extrusion between the original and the new arc length is approximately 2.00 %.

If we want to maintain uniform coverage as the diameter of the object to be printed increases, we must increase the extrusion by a certain percentage (in this case, by 2 %) for each subsequent layer, starting with the second, assuming the first layer is constant, and the extrusion is equal to calculated with the slicing program and adds up to 100 %.

The result of setting the manual filling factor in comparison with the unregulated material flow is shown in Fig. 5.11. According to the results of the test print, it can be concluded that a manually set percentage of the beginning gives a larger amount of material, but after increasing the number of layers, the amount of material remains smaller than what is needed for further printing.

Fig. 5.11. Example of cylindrical printing without flow control and with manual percentage.

To ensure a dynamic change in the flow coefficient, a Python code (Appendix 3) has been created, which processes the G-code file and changes the extrusion parameter for each layer separately (Appendix 3). The coefficient is calculated based on the arc length and flow coefficient of each previous layer. The total flow coefficient is calculated separately and displayed during code processing; an example of percentage filling for a 32 mm diameter cylinder is shown in Table 5.2.

Table 5.2

Dynamically Changing Material Extrusion Ratio Example Using Python Code

Layer number	Percentage change in layer	Overall percentage change
1	0.0 %	0 %
2	1.96 %	1.96 %
3	1.92 %	3.88 %
4	1.89 %	5.77 %

5.2. Development of a 3-axis FDM cylindrical coordinate system printer prototype

The first stage in the creation of the prototype is to prepare a 3D CAD concept of the prototype (Fig. 5.12), which is modeled in the Autodesk Fusion 360 application, where the location of all elements is specified. The list of components to be used for creating a prototype is shown in Table 5.3.
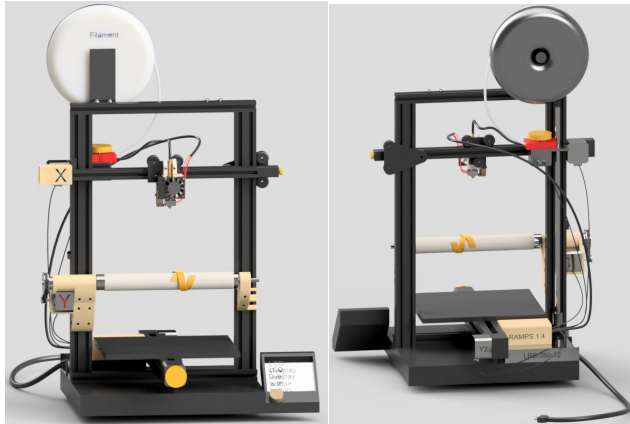

Fig. 5.12. CAD model of a cylindrical 3D printer prototype created in Autodesk Fusion 360.

Table 5.3

List of Components to Be Used for a 5-Axis Cylindrical FDM 3D Printer Prototype

Title	Model	Parameters
3D printer	Creality Ender-3 V2	CoreXZ Cartesian FDM 3D printer
Stepper motor	2 × NEMA 17 42-34 BJ42D15-26V12 2 × NEMA 17 42-40 42HS040DF260A	Pitch angle: 1.8°, nominal current 0.8 A, 1.0 A number of phases: 2, torque: 0.8 Nm
Stepper motor driver	4 × A4988	Operating voltage: 8–35 V DC, logic voltage: 3–5.5 V DC, Imax 2 A
Power supply	Meanwell LRS-350-12	12 V DC, 350 W, 27 A, 48–63 Hz
Control elements	Arduino Mega 2560, RAMPS 1.4	ATMega 2560 16 MHz
Transmission mechanism	1 × 2GT 20 tooth gear, 1 × 2GT 60 tooth gear 1 × 2GT-6 218 mm timing belt, 2 × 688ZZ bearings, 400 mm × 8 mm threaded screw	Gear ratio 3:1
Software	Marlin	Control of the prototype can be realized using a Web interface with Wi-Fi protocol
3D printing materials	Creality PA12 white 1.75 mm	The printhead elements and Y-axis body are printed

The body of the prototype is made of 4020 and 2020 aluminum profiles, which ensures the stability of the print and, accordingly, the low weight of the axles.

The print head is designed and positioned to offer as much space as possible between the cylindrical print table and the print head elements, ensuring that the print head elements do not come into contact with the elements of the printed objects.

A NEMA 17 42-40 step motor is responsible for lifting the Z-axis, to which an 8 mm diameter (2 mm pitch, 8 mm lead) and 400 mm long threaded screw is attached to the X-axis fastening elements. The X-axis is mounted on a 2020 aluminum profile and is controlled using a NEMA 17 42-34 step motor with a GT2 20 tooth gear and a GT2 6 mm thick and 750 mm long belt attached to the print head mounts.

Timing belt tension can be set using the axle-mounted tension adjustment mechanism. The Y-axis consists of a cylindrical printing table consisting of a metallic 8 mm diameter 400 mm long threaded rod, which provides the possibility of using the entire printing length of the X-axis, two 8 mm thick 22 mm diameter 686zz bearings, a transmission system of GT2 60 tooth and GT2 20 tooth gears connected to 218 mm long GT2 6 mm thick belt, inserted in a modeled and printed nylon case.

For the production of the prototype, it was necessary to create mechanically and temperature-resistant elements up to 150 °C for fastening the print head and cylindrical table, which were printed with the traditional FDM method using Fiberlogy nylon PA12 white sharp filament (Fig. 5.13).
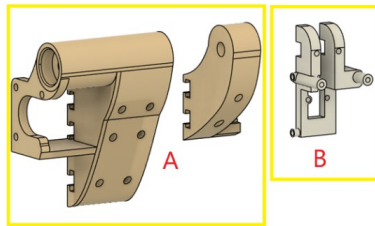

Fig. 5.13. CAD model of traditional FDM printed PA12 nylon cylindrical print table, stepper motor and screw rod (A) and printhead elements (B) mounting.

The prototype cylindrical print table mounting features a CAD-modeled mounting body that is printed from Fiberlogy PA12 in a white crisp nylon filament that provides high resistance to mechanical stress. In order to ensure the concentricity of the Y-axis, an additional bracket has been created on the other end of the Y-axis, and an automatic leveling probe has been added to determine and adjust the position of the cylinder. To ensure quick switching between flat and cylindrical printing, a Y2-axis with the flat table controlled by a NEMA 17 42-34 step motor is located, and a position sensor is located next to the motor for determining the minimum position of the Y2-table [26]. All control and management elements are connected to the Arduino Mega 2560 control board with the RAMPS 1.4 expansion board, which is connected to a 12V DC 29A pulse power supply unit placed on the base of the 3D printer. To control the printing process and receive information about the printing progress, an LCD 12864KBA screen with a control button is connected. G-code can be loaded onto a 3D printer prototype

memory card using a USB connection to a personal computer or using portable SD memory card media [27].

The RAMPS 1.4 expansion board is mounted on top of the Arduino Mega 2560 microcontroller board, and all elements of the 3D printer prototype are connected to the RAMPS 1.4 expansion board. The prototype uses two NEMA 17 42-34 stepper motors on the X- and Y-axis, two NEMA 17 42-40 stepper motors on the E- and Z-axis, four A4988 stepper motor drivers installed, three position sensors, three NTC 100K type thermistors, prints table, the ceramic heating element of the print head, and two cooling fans; speed control is provided for the cooling of the printed objects in the output D9 of the print head, but it cannot be adjusted for the cooling of the radiator of the print head in the 12V-AUX output; accordingly, it is necessary to use two separate DC/DC converters, power supply connected from a 12 V DC power supply unit. The connection of the elements can be seen in Fig. 5.14.
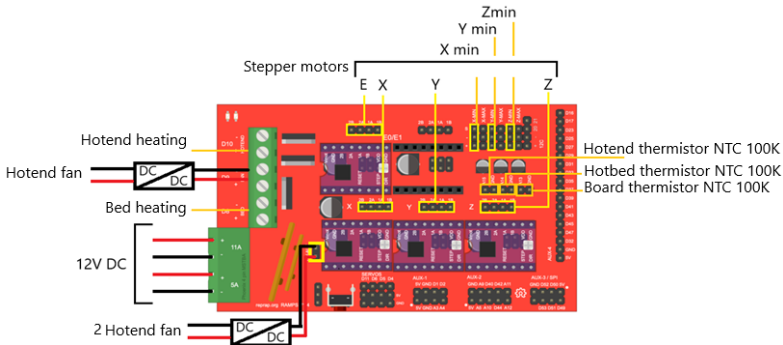

Fig. 5.14. Connection diagram of prototype elements.

Cylindrical printing table structure consists of two (Fig. 5.19) nylon fastening elements, three 686zz bearings, 8 mm diameter 400 mm long threaded steel rod, 2GT 60 and 20 tooth gears, 2GT 218 mm tooth belt, nylon printed cylindrical 31 mm diameter base with 8 mm diameter threaded hole and hollow steel cylinder 32 mm in diameter and 0.5 mm thick, which ensures surface smoothness and precision. The steel cylinder is not intended for heating because its surface needs to be covered with an adhesion material, such as varnish, glue or paper-painting tape, which was used in the tests. The assembled structure can be seen in Fig. 5.15 [28].
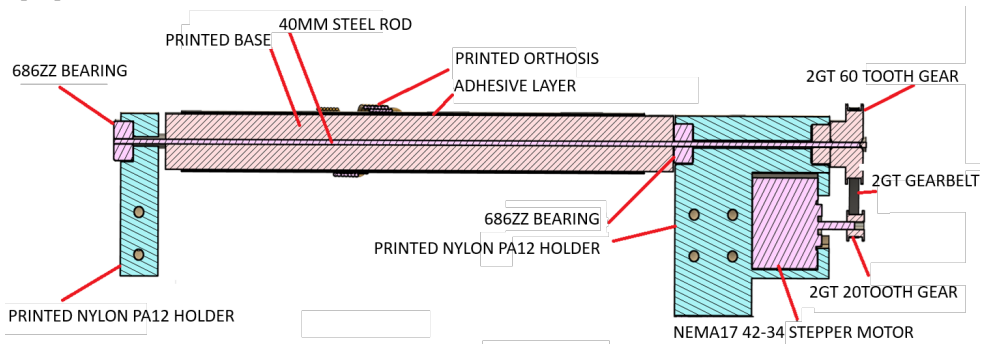

Fig. 5.15. Section of the cylindrical construction of the printing table.

The cylindrical print base of the table is printed on a traditional FDM 3D printer using nylon PA12 filament. The size of the base can be adjusted by changing its diameter and by changing the size and diameter of the printing table accordingly. It is possible to print immediately on the printing base if it is covered with a removable adhesive layer, however, to ensure the smoothness of the cylinder and prevent changes in geometry due to the influence of high temperatures, an additional 0.5 mm thick steel cylinder has been used.

The created and assembled prototype (Fig. 5.16) is connected to a 230 V AC power source and a TENMA oscilloscope to read voltage and current parameters and perform consumption calculations.
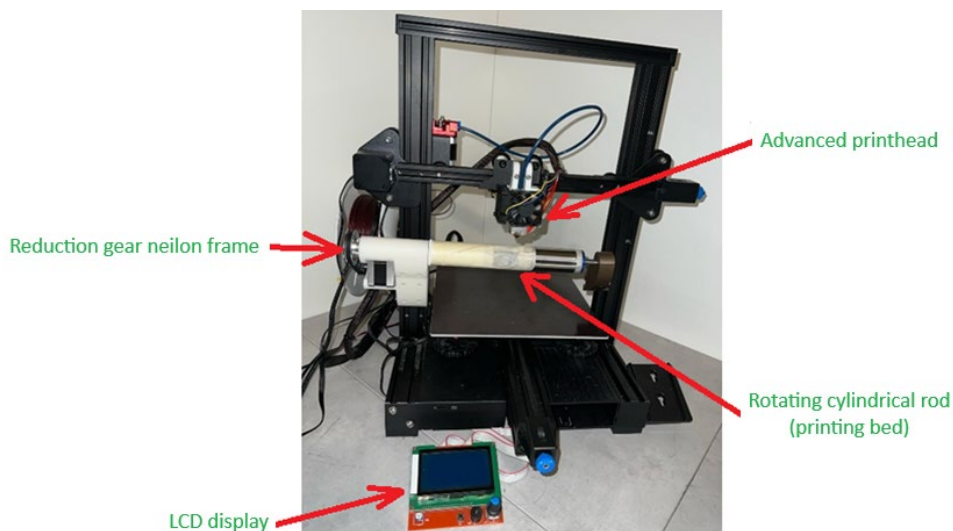

Fig. 5.16. Cylindrical printing prototype.

Marlin firmware is selected for the control board. Marlin provides code written in C with several settings files. To load the Marlin software onto the control board, it is connected to a PC via a USB cable through the COM port. The program offers many settings and the ability to connect multiple axes and other control devices.

The code is compiled in the Arduino IDE and stored in the memory of the Arduino Mega 2560 control board. The generated G-code, pre-prepared for printing, is written to the SD memory card and inserted into the connector of the LCD screen. The stages of orthosis manufacturing and the stages of software preparation are shown in the diagram (Fig. 5.22).

To ensure high printing accuracy, it is necessary to determine the concentricity of the printing table. The automatic height sensor for the CR-Touch 3D printer is used to detect this. The sensor is mounted on the print head next to the print nozzle. This sensor is designed to determine the geometry of the flat printing table surface, and the test method is based on the fact that when the sensor contacts the surface, it registers it as a signal and transfers this information to the control board. Based on the received data, the control panel determines the height and unevenness of the table (Fig. 5.17). Prior calibration is required for CR-Touch to function properly. This includes adjusting the height of the sensor and its distance from the

nozzle to ensure optimal contact with the table surface. In the Cylindrical 3D prototype, this sensor is used similarly to a flat-bed 3D printer. The print cylinder is divided into zones, and during the test, the cylinder rotates and the sensor determines the distance from the nozzle to the cylinder. In this way, the arrangement of the cylinder in the space is obtained and the position of the cylinder can be mechanically corrected by changing the arrangement of the fastening elements on the metallic profiles of the printer. If all the distances are the same or similar after determining the position with the sensor, it can be determined that the axle is positioned correctly and has good concentricity along the entire length. If, when changing the position of the axis or when measuring, the printing table still causes the distances along the entire length of the axis to not match, then the axis has bad concentricity, and its elements need to be replaced.
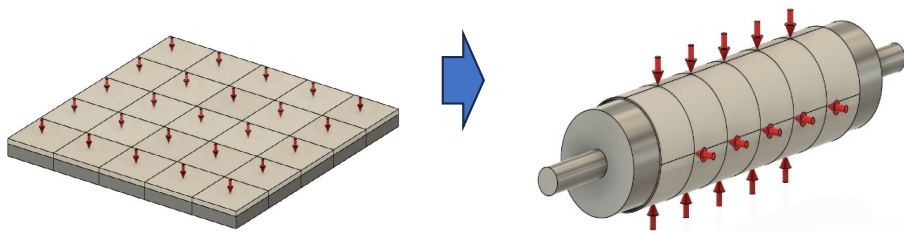

Fig. 5.17. Method of cylindrical table position determination and concentricity test.

Settings and preparation for printing in the software

Before starting printing, it is necessary to calibrate the stepper motors. The step engine needs to specify the number of steps per millimeter. This is necessary to ensure that the stepper motors are cut to the required specified distance. The Y-axis is equipped with a transmission mechanism in the ratio of 3:1; due to this, it can be predicted that the number of steps per millimeter will be three times higher; however, after the calibration, it was found that a larger number of steps is needed than predicted. After calibrating all stepper motors, the following settings have been made:

- X-axis: 80 steps per mm;
- Y-axis: 260 steps per mm;
- Z-axis: 400 steps per mm;
- E-axis: 93 steps per mm.

The next step is to set the maximum allowable velocity, acceleration and angular velocity. Based on the parameters of the kinematics of the 3D printer and Ender 3 V2, the following parameters are set for the cylindrical prototype:

- X-axis: Max speed: 100 mm/s; max acceleration: 500 mm/s^2; max angular speed: 5 mm/s;
- Y-axis: Max speed: 100 mm/s; aax acceleration: 500 mm/s^2; max angular speed: 0.3 mm/s;
- Z-axis: Max speed: 5 mm/s; max acceleration: 100 mm/s^2; max angular speed: 5 mm/s;
- E-axis: Max speed: 25 mm/s; max acceleration: 1000 mm/s^2; max angular speed: 5 mm/s.

Maximum print head temperature is limited to 260 °C, and maximum Y2 print table temperature is 100 °C.

5.3. Prototype testing of a 3-axis FDM 3D cylindrical printer

Description of testing methodology for a 3-axis FDM 3D cylindrical printer prototype

Based on the sources [29], [30], [31], the sizes and shapes of the test samples have been selected. For testing the mechanical strength of the printed objects, 3D CAD cylinder models have been created, which are 100 mm long with an initial diameter of 32 mm and a thickness of 1.5 mm. According to the given parameters, the outer diameter of such samples is 35 mm. The models were printed by placing the models in three different positions. The first option is to place the layers so that they are printed in one axis direction, Z; the second option is to print the models by placing them in the XY direction; such theoretical models will not differ from the test creatures because the mechanical strength of the material will be tested.

The third option for a cylindrical prototype is to print the model by changing the filling angle in the XY direction (Fig. 5.18). In this way, at 0°, we test the adhesion of the material; at 90°, the strength parameter of the material; and at 45°, a sample of cylindrical printing, which can be compared with the two previous variants. The angle is set at 45°, which theoretically corresponds to greater durability. In order to make sure that the results are directly caused by the adhesion of the layers and not the properties of the material, test models with different layer thicknesses (0.1 mm, 0.2 mm, 0.3 mm) and temperatures (220 °C, 230 °C and 240 °C) have been printed. During the temperature increase, the material remains in a liquid state for a longer time, respectively the layers adhere to each other better; however, by increasing the temperature, the material degrades faster, therefore cylindrical printing can theoretically increase the mechanical strength of the printed objects without reducing the properties of the material. Fiberlogy PLA and PET-G and Rosa3D PLA and PET-G white have been used for printing 1.75 mm filaments. The models are prepared in PrusaSlicer 2.7.1 and Ultimaker Cura 5.2.0. The UV-curable resin samples are also printed on the Anycubic Mono SLA 3D printer. This is why the resin is not printed with temperature and layer parameters, only one sample participates in the tests.
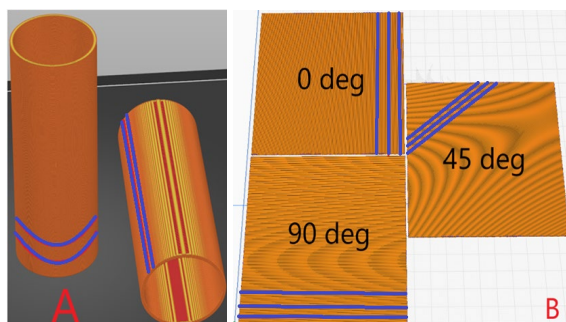

Fig. 5.18. Layout of the test 3D CAD model for printing on flatbed (A) and cylindrical (B) printers.

Flexural strength testing

A 3-point test bench is used for testing the flexural strength of the printed test samples, where two points are the support material, and the third point is the place where the load is applied (Fig. 5.19). This test is used to determine the modulus of elasticity, flexural strength and other mechanical properties of a material. Samples of materials should be made in accordance with the relevant standards or requirements. Usually they are rectangular in shape and have certain dimensions. Usually, sample sizes are 50–200 mm in length, 10–50 mm in width and 2–10 mm in thickness; however our occasional printed samples are 100 mm in length, 35 mm in width and 1.5 mm in thickness. An Instron 5965 test bench is used for flexural strength testing [29], [30], [31].
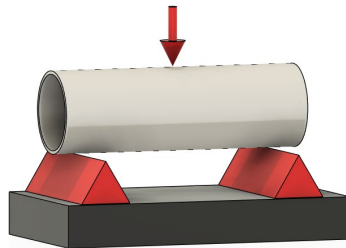

Fig. 5.19. Schematic of the flexural strength testing bench.

Izod impact testing

The second test tested the Izod impact resistance of the printed samples. For testing, it is necessary to create a breaking point of a certain size in the middle of each sample. Accordingly there are printed samples with a breaking point. Testing is done by placing the sample in a vice and hitting it at a speed of 1.5–2 m/s with a hammer attached to the stand with a mass of 0.67 kg, and based on this, it can be determined how much energy the test sample has absorbed. CEAST Resil impactor bench [32] is used for Izod impact tests.

Recording of current and voltage and determination of electricity consumption

The main purpose of the power consumption test is to compare the efficiency of two different control system configurations for a cylindrical prototype 3D printer: a standard Arduino Mega combination with A4988 drivers and a more advanced BigTreeTech Manta M8P system with TMC2209 drivers. The purpose of the test is to see if replacing the control board and drivers reduces energy consumption while keeping the same set of connected elements, including the heated table, which may indicate an improvement in the energy efficiency of the updated system. Two systems have the same number of elements connected, ensuring the same load. However, individual types of stepper drivers have different operating currents, and in order to ensure a comparison of the energy management efficiency of the systems, it is necessary to provide the same initial settings, so it is first necessary to determine the maximum current of the stepper motors on the coils, which is 1 A for both selected stepper motors. The safety factor is assumed to be 0.7. Then the rms operating current on the coils for A4988 and

TMC2209 is calculated according to Formula (4.8). For A4988 drivers, the operating current is adjustable with an adjustable resistor on the driver itself, but for TMC2209, the current is specified in the firmware of the control board and by adjusting the reference voltage V_{ref}, which is calculated according to Formula (5.13).

$$I_{rms} = I_{max} \times 0.7, \qquad (5.13)$$

where I_{rms} is the rms operating current on the coils, A; I_{max} is the maximum current of the stepper motor on the coils, A.

$$V_{ref} = I_{rms} \times R_{sens}, \qquad (5.14)$$

where V_{ref} is the reference voltage of the driver, V; I_{rms} is the rms operating current on the coils, A; and R_{sens} is the resistance of the driver resistor, Ω.

After all calculations, $V_{ref} = 0.80$ V and $I_{rms} = 0.71$ A are set for A4988 driver and $V_{ref} = 1.00$ V and $I_{rms} = 0.70$ A for TMC2209 driver.

To ensure the same stepper motor parameters, stepper motor temperature and operating volume parameters were determined using a non-contact infrared (IR) thermometer Wintact WT700 and a sound level meter, Sound Bee TFA. 60.0 dB from 1 meter distance and 50.0 °C on X- and Y-axis stepper motors were assumed as reference settings corresponding to the most heavily loaded motors [33].

A data acquisition system based on an Arduino Uno development board with an ATmega328 microcontroller was created to collect information on voltage, current and consumed electricity. This board is compact, easy to program and provides all the necessary functions. An Allegro ACS712 20 V DC current transducer is additionally used for current measurements, as the maximum printer current is expected to be 14.5 A. The connection diagram of current measurement components is shown in Fig. 5.20. The control board is powered by a 5 V 1 A power supply unit [34], [35], [36].
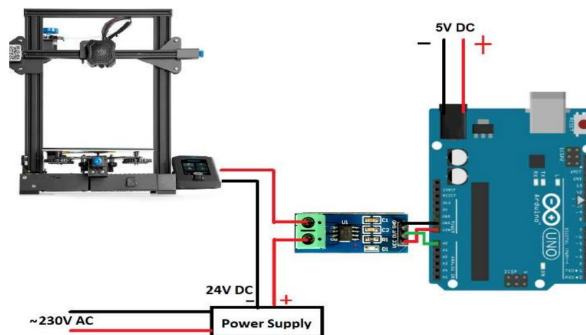

Fig. 5.20. Connection diagram of current measurement system elements [37].

For voltage measurements, a voltage divider circuit has been created, which is also connected to the same Arduino Uno control board using the connection of two resistors to 100 kΩ and 1 MΩ (Fig. 5.21). Such a circuit divides the input voltage by a ratio of 1 to 11 and

gives the possibility to effectively measure the voltage up to about 50 V DC, which is also necessary because 12 V and 24 V power sources are used. Voltage and current measurements have been made on the DC connection terminals of the pulse power supply unit. The accuracy of the ACS712 current transducer is 100 mV per 1 A, and the accuracy of the voltage divider is estimated to be around 4–5 %. A digital multimeter MASTECH M832 with an accuracy of 2 mA current and 0.1 mV voltage is used to check additional results [38], [39], [40], [41].
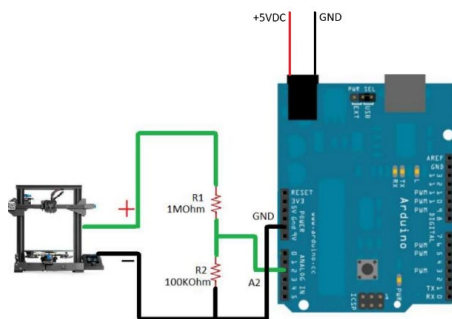

Fig. 5.21. Connection scheme of elements of the voltage measurement system [37].

5.4. Results

Prototype testing of a three-dimensional cylindrical coordinate system printer

Each test has three test samples printed for each parameter. The test results of the dependence of the maximum bending load on the arrangement of the layers and the printing temperature at temperatures of 220 °C, 230 °C and 240 °C and at layer thicknesses of 0.1 mm, 0.2 mm and 0.3 mm are summarized in Graphs 5.22, 5.23. and 5.24. Impact tests are summarized in Figs. 5.25, 5.26, 5.27.
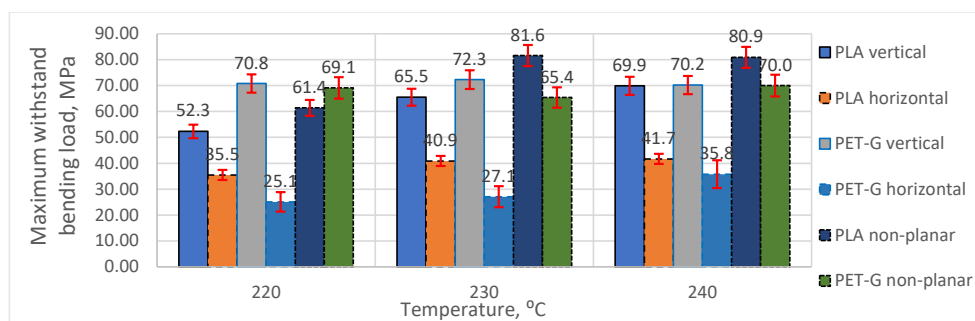

Fig. 5.22. Maximum withstand bending load depending on layer arrangement and printing temperature at 0.3 mm layer thickness.

Fig. 5.23. Maximum withstand bending load depending on layer layout and printing temperature at 0.2 mm layer thickness.

Fig. 5.24. Maximum withstand bending load depending on layer arrangement and printing temperature at 0.1 mm layer thickness.

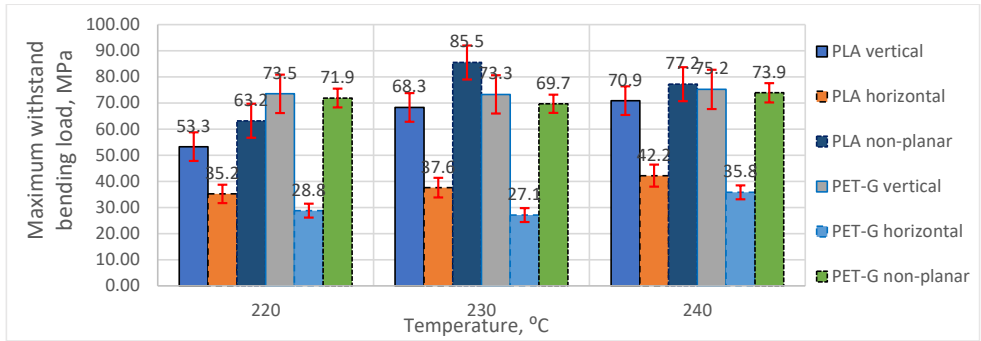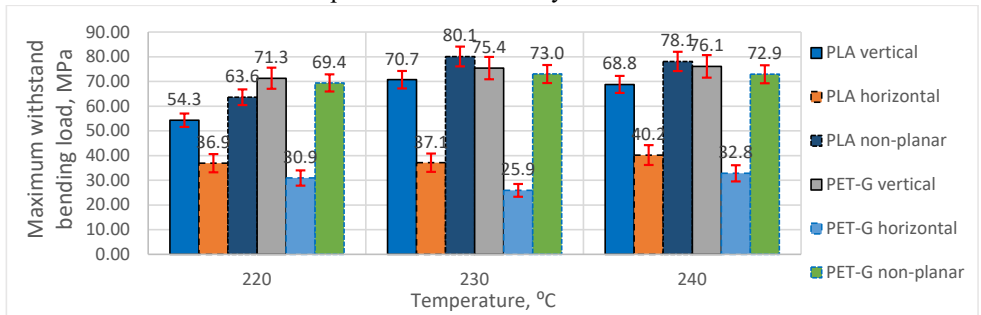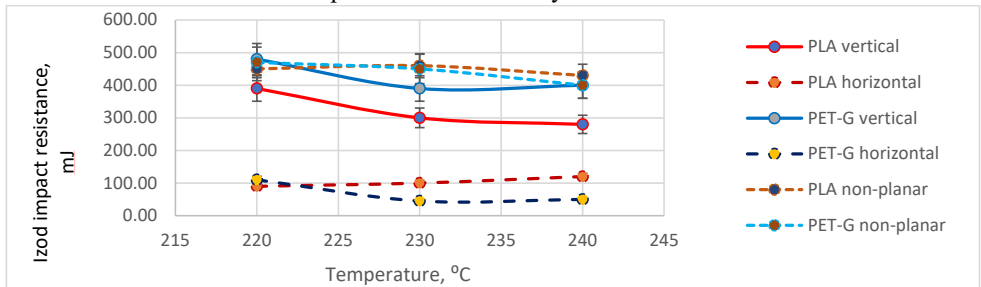Fig. 5.25. Maximum impact resistance depending on layer arrangement and printing temperature at 0.3 mm layer thickness.
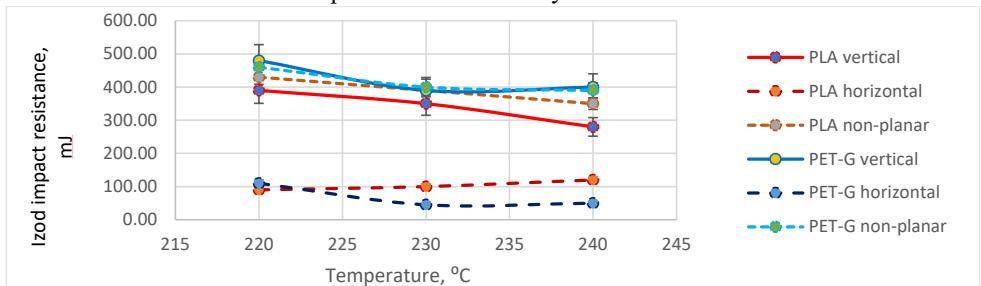

Fig. 5.26. Maximum impact resistance depending on layer arrangement and printing temperature at 0.2 mm layer thickness.
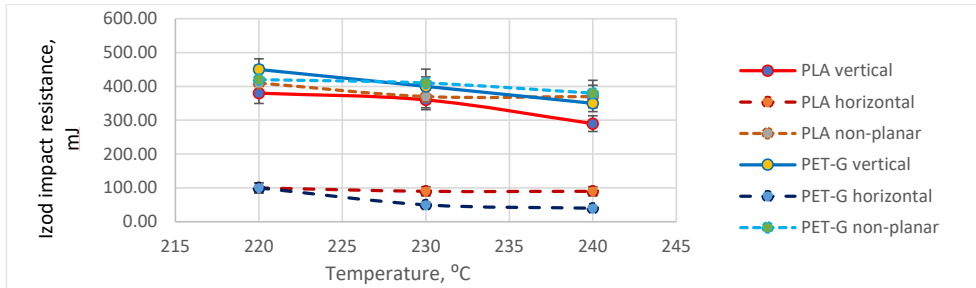
Fig. 5.27. Maximum impact resistance depending on layer layout and printing temperature at 0.1 mm layer thickness.

Determining print accuracy

Print sizes of flat (white) and cylindrical (ruby) Fiberlogy PLA and PET-G material test samples are compared. The width, length and thickness of the samples have been compared (Fig. 5.28). The dimensions of the model in the CAD program are 100 mm in length, 35mm in diameter and 1.5 mm in thickness. Based on the printing parameters of PLA materials and the fact that the material has 0.2–0.3 % shrinkage, real PLA printed samples are expected to be correspondingly smaller to about 0.25 %. Approximate shrinkage of PET-G material is expected to be 0.5–1.5 % of the limit. Dimensions are measured with a digital caliper Parkside HG08763A with an accuracy of 0.01 mm.

Fig. 5.28. Comparison results of printed sample sizes of PLA material.

Material flow control test

Fiberlogy PLA ruby filament is used for material flow comparison. Based on this, as the height of the layers increases in cylinder printing, the arc length of the printing cylinder also increases, and it is necessary to regulate the material flow. A CAD model has been created with an initial diameter of 32 mm and a layer thickness of 30 mm, which will result in an outer diameter of 92 mm. The first test print is made without material flow changes; the second print is a manually set flow increase percentage of 1 %, where this percentage is taken care of in each subsequent layer. A third test has been performed, with material flow regulation using Python code and based on previously performed calculations. All three samples are shown in Fig. 5.29.
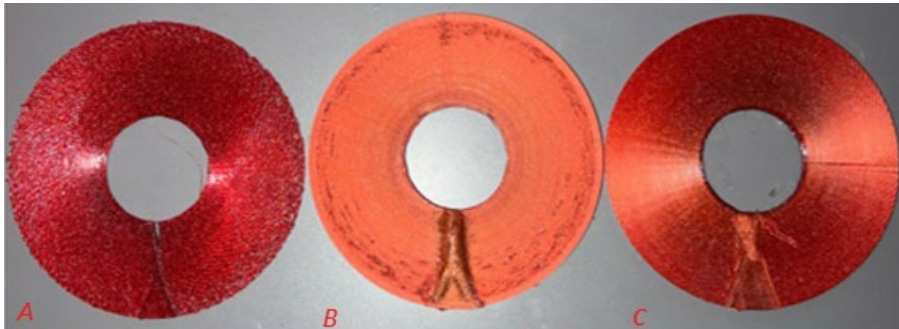

Fig. 5.29. Flow adjustment test: A – sample without adjustment; B – manually set percentage; C – sample with flow adjustment by changing G-code commands.

SUMMARY OF RESULTS OF NON-LAYERED 3-AXIS 3D PRINTING METHOD

In bending samples with a thickness of 0.3 mm, it was found that depending on the arrangement of the layers, the bending strength of the final product can vary by an average of 67–266 %, so the samples in which the layers are located horizontally relative to the printing table have lower strength than the samples in which the layers are located vertically. At the same time, for samples produced in cylindrical form, the PET-G material performed on average the same or 10 % worse than the vertical samples and up to 18 % stronger than the PLA material.

When comparing samples with a thickness of 0.2 mm, the strength of all samples remained the same or increased up to 4.7 % compared to the 0.3 mm samples. The strength of the cylindrical samples varied from –4.5 % to 6.5 % on average. Comparing the 0.1 mm samples with the 0.3 mm samples, the strength varied from –3.4 % to 11.6 %. In the standard samples, as the layer thickness decreased by 0.2 mm, the strength changed from –2.9 % to 3.5 % and from
–1.5 % to 8.4 % for the 0.1 mm samples. On average, for our specific PLA material, an increase in temperature increased the adhesion of the layers to each other, while for the PET-G material, the flexural strength remained virtually unchanged. At the same time, the samples printed using the cylindrical method performed the same or better than the vertical samples, probably due to a more even distribution of the load since the layers were filled at an angle of 45° and each subsequent word was rotated 180° relative to the previous layer, so the layers intersected and formed a stronger structure than just vertical layers. In addition, the printed samples of UV resin have been tested to compare the capabilities of different technologies, and according to the results, the UV curing resin samples showed an higher impact strength of 650 mJ and a bending strength of 38 MPa, which on average corresponds to 35–66 % higher impact strength compared to better PLA and PET-G samples, but 42–44.5 % lower bending strength.

Comparing exactly how the samples were damaged during bending, it is clear that the horizontal samples (A) clearly break along the layer print line, while the cylindrical samples (B) break over the entire surface of the sample, distributing the load evenly (Fig. 5.30).
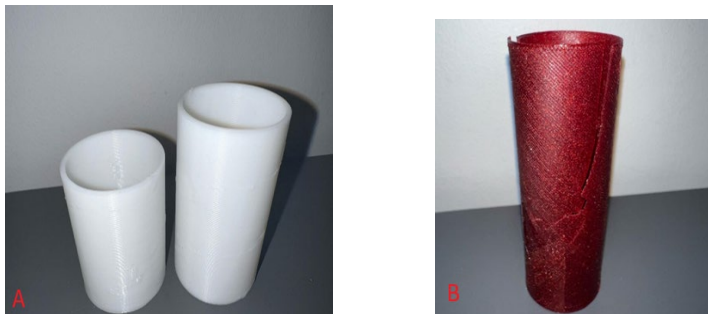

Fig. 5.30. Flexural test specimen failure examples: A – example of horizontal layers; B – example of a cylindrical method.

Horizontally printed samples of PTE-G material with a layer thickness of 0.3 mm at a temperature of 220 °C, which is the minimum printing temperature for this material, turned out to be the worst. This specimen was subjected to a bending load of 25.1 MPa. The best result was shown by a cylindrical PLA sample printed at a temperature of 230 °C with a layer thickness of 0.2 mm and withstanding a load of 85.5 MPa. For this PLA material from the manufacturer Fiberlog, 230 °C is the maximum allowable temperature for printing and, as it turns out, provides the greatest durability.

The samples performed differently in the impact tests, and almost all samples became less durable as the temperature increased, which can be explained by the fact that the material became more brittle and inflexible as the printing temperature increased. The weakest sample turned out to be a 0.3 mm thick sample pressed horizontally at a temperature of 230 °C, withstanding a load of 45 MJ. The most resistant was the PET-G sample with a thickness of 0.2 mm, printed vertically at a temperature of 220 °C. However, the cylindrically printed PLA and Pet-G samples were able to withstand a load of 460 MJ and 470 MJ, respectively, which, given the measurement accuracy of ±5 %, is almost identical and may depend on the accuracy. measurements. Thus, cylindrical printing is the most advantageous option, as it provides an average of 6.5–11.6 % more bending-resistant products and comparable impact resistance compared to vertical printing.

Comparing the printing accuracy, the samples printed by the conventional method showed an average of 0.7 % smaller parameters than those specified in the CAD model, which can be explained by material shrinkage. At the same time, the thickness of the layer turned out to be 3 % higher, which is explained by the accuracy of setting the thickness of the print line and the accuracy of the printer itself and the nozzle used.

The cylindrical sample turned out to be, on average, 1 % larger in all aspects, which is explained by the accuracy of the settings of the printer and its components.

Comparing the methods of regulating the flow of material, it is clearly seen that if the flow is not regulated, voids are formed in the sample after a few rounds, and the amount of supplied material is insufficient. The resulting sample is porous and absolutely unstable to any type of load, since the layers are practically not connected to each other. The connection seam is practically invisible.

When manually setting the percentage of filling, hanging material appears at the beginning of printing, the filling normalizes in the middle of the sample and approaching the highest layers, porosity appears, and the layers begin to connect more weakly with each other. Also, the seam connecting the layers during full rotation becomes clearly visible, and a sag appears. Using the controlled feeding method, using G-code processing using Python code, the filling is smoothed, there is no porosity, and the seam becomes almost invisible.

6. FIVE-AXIS 3D PRINTING SOLUTION FOR PRINTING OF COMPLEX-SHAPED ORTHOSIS

6.1. Development of a 5-axis cylindrical non-layered 3D printer method

An orthosis is usually a device adapted to the anatomy and intended to immobilize, support or correct certain conditions. The orthosis can vary from a simple plate construction to more complex ones with joints and fixation elements.

For comparison of quality and parameters, an example of orthosis has been selected – a finger splint for fixation of the distal phalanx joint, ARmedical AR-061 variant (Fig. 6.1). If we consider the shape of the orthosis as an example, the finger orthosis usually has a cylindrical or semi-cylindrical shape, which corresponds to the contour and size of the finger. The design can be quite simple, consisting of a mouth guard, or more complex, with moving parts to limit or allow a certain amount of movement.

If you take into account more complex options, for example, hand orthoses, then their printing is more difficult since they must support not only the wrist but also partially the forearm and hand. It can be a curved splint that wraps around the wrist and forearm to provide rigidity and support. Sometimes slits or adjustable straps are included for a better fit. Printing a wrist mount can present some challenges due to its more complex shape and dimensions, which may be beyond the capabilities of a cylindrical printer. Depending on the design of the orthosis, print supports may be required, which may be more difficult to implement.

Fig. 6.1. Orthosis example, hand finger splint for distal phalanx joint fixation ARmedical AR-061.

The main advantage of the prototype to be developed is the fast switching of printing modes, where by switching the axis wires, you can quickly switch between traditional printing mode, three-axis cylindrical printing and five-axis cylindrical printing.

The idea of the 5-axis prototype is based on the fact that when a CAD model of a human limb is modeled, the necessary part on which the orthosis will be applied will be printed as a base, which will be mounted on a rotating 8 mm diameter rod. As a result, a rotating base will be obtained on which the orthosis model will already be printed; in this way, the support material will be realized, which will be covered with an adhesive material (paper masking tape), which can be easily separated from the orthosis. In the 5-axis solution, the scheme is shown in Fig. 6.2.
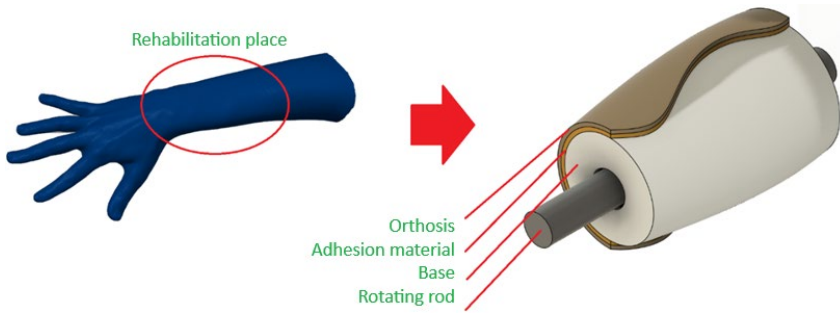
Fig. 6.2. Defining and transforming the rehabilitation site from a CAD model into an orthosis placement on a rotating base.

As an example of how a non-planar 3D printing path is made with a variable filling direction angle, an example of a cube model is described, where the stages of generation of a non-planar path are depicted (Fig. 6.3). In the first stage, it is necessary to use some space where the object will be placed for its further slicing. Two equal square planes are used for such a space, where one plane is directly above the other plane.
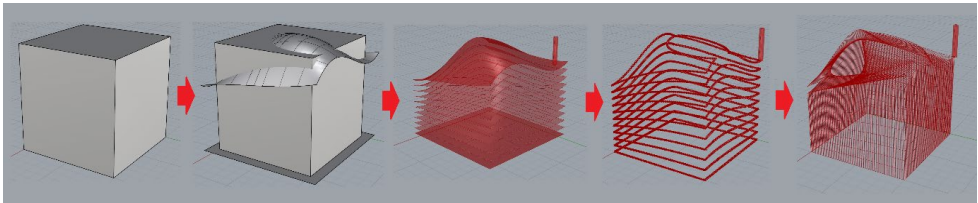

Fig. 6.3. Model interpolation and perimeter and fill path creation in Rhinoceros 3D Grasshopper extension.

The lower plane represents the print base on which the object will be printed, while the upper plane is needed to control the shape in which the object to be cut will be cut. The shape of the upper plane can be adjusted and adapted to your needs, for example, it can be used to adjust the pressure distribution of the orthosis and the way in which the orthosis will be printed.

The next step is to use interpolation by multiplying the number of planes using the tween function; the distance between the generated planes and their amount determines the height of the print, and the more layers that will be generated, the thinner the object will be sliced. When the interpolated layers are placed using the path function, a continuous spiral path is generated between the layers with flow from the bottom layer to the top. However, only a rough path of the perimeter of the object has been generated in this way, and two more planes have been used to create the fill path, which are placed at a certain angle to the edges of the existing planes; the angle between the edges of the horizontal planes and the edges of the vertical planes determine the angle of the fill, and to get as much as possible horizontal filling, planes of stronger parts are placed at an angle of 45°. Using the previous stages, one spiral path is repeatedly generated [42], [43].

The result is a file with points with coordinates that can be used for G-code generation. The path of all non-planar method operations in the Grasshopper visual development environment is shown in Fig. 6.4.
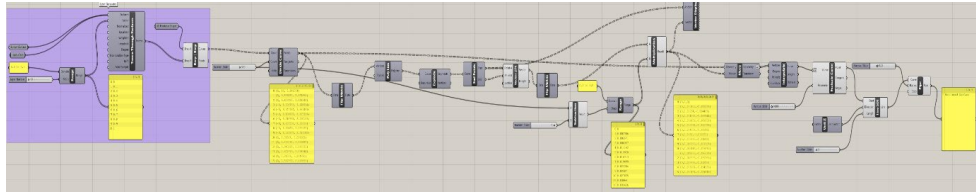

Fig. 6.4. Control code for model slicing and path creation in the Grasshopper extension of Rhinoceros 3D.

A 5-axis printing mechanism is embedded inside the Grasshopper environment to accurately simulate the movement of all axes. The limb shape-based base and printable orthosis files are loaded separately, and the motion of the 5-axis prototype is simulated (Fig. 6.5). Movements are transformed into G-code commands using a control code written in Python, in which all the necessary parameters are entered (velocities, accelerations, axis coordinates, required amount of material feed, placement on the control board, and others).
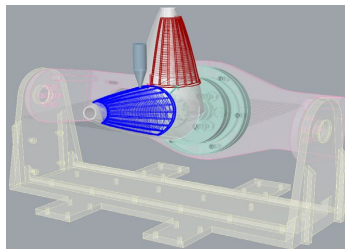

Fig. 6.5. Simulation of the movements of a 5-axis 3D printer prototype in Rhinoceros 3D.

6.2. Development of a 5-axis cylindrical non-layered 3D printer

In order to print more complex structures while maintaining the possibility of cylindrical printing by changing the fill angle at any angle of the printed product, an open-source solution was needed to develop a multi-axis solution. The Open5X project, founded in 2022, previously mentioned by F. Hong [43], is taken as the basis of the multi-axis prototype. This 5-axis solution offers the printer the ability to add two more axes for additional degrees of freedom, which in turn allows for more complex shapes to be printed. The Prusa i3 Descartes CoreXZ kinematics 3D printer is taken as the basis of the project, which has additional connected axes controlled by additional stepper motors; as a result, it is necessary to control five separate axes simultaneously. Additional axes are implemented as a rotary table, which is mounted on another rotary axis, which in turn is attached to the Y-axis of the printer. The basis of the project is a visual code development environment in the Rhinoceros 3D program, which simultaneously uses the Grasshopper and Puffer Fish extensions. In a visual environment, a code has been developed and simulated that replaces the non-planar method slicing program and simulates the control of the printer elements inside the program. However, this solution has limitations

that collide with the difficulty of non-flat code generation, including printing only the model perimeter without including the model fill and the absence of several necessary functions, such as perimeter and fill angle adjustment and line thickness adjustment. It is not possible to use overlaying layers and variable filling angles; however, a non-flat slicing solution is used, which gives the opportunity to print model elements by turning the model to the required position (Fig. 6.6) [44].
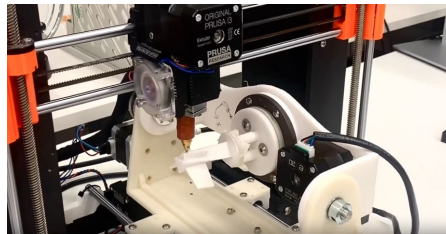

Fig. 6.6. Open5X multi-axis 3D printer project [43].

In order to adapt cylindrical printing to a 5-axis solution, additional improvements have been made to an existing prototype configuration. Firstly, in order to increase the number of axes, it is necessary to use a greater number of stepper motors; each axis has a separate stepper motor and together with the printhead material supply motor, it is necessary to connect six separately controllable stepper motors. For this purpose, a pre-selected Bigtreetech Manta M8P 2.0 control board based on an STM32H723ZET6 microcontroller with a 550 Mhz speed and the ability to connect up to 8 separately controllable stepper motors has been used. An additional expansion board Raspberry Pi CB4 using the Klipper control program has been used to enable control of the prototype without the use of a display and control using the WiFi protocol. Additional axes use NEMA 17 42-34 stepper motors, which are lighter than NEMA 17 42-40 stepper motors and provide the necessary torque. $6 \times$ TMC2209 stepper motors connected using the UART protocol have been used because their use provides a sharp position determination option without the use of end position sensors. Based on the fact that additional stepper motors with drivers have been added and the Manta M8P board has the possibility to connect both 12 V and 24 V power supply, the new 24 V Mean Well LRS-350-24 power supply unit has been selected, with a maximum power of 350 W 14.6 A. The Klipper firmware is loaded onto a MicroSD memory card inserted into the Manta M8P control board. The connection of all elements is shown in Fig. 6.7.
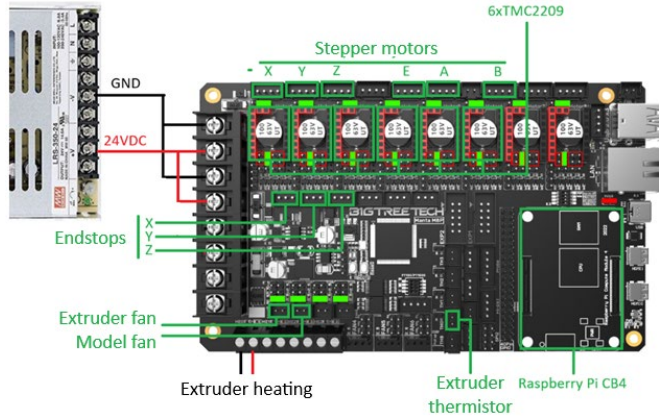
Fig. 6.7. 5-axis 3D printer prototype element connection diagram.

The list of components to be used for a 5-axis cylindrical FDM 3D printer is shown in Table 6.1.

Table.6.1

List of Components to Be Used for a 5-Axis Cylindrical FDM 3D Printer Prototype

Title	Model	Parameters
3D printer	Creality Ender-3 V2	CoreXZ Cartesian FDM 3D printer
Stepper motor	4 × NEMA 17 42-34 BJ42D15-26V12 2 × NEMA 17 42-40 42HS040DF260A	Pitch angle: 1.8°, nominal current 0.8 A, 1.0 A, number of phases: 2, torque: 0.8 Nm
Stepper motor driver	6 × TMC2209	Operating voltage: 8–35 V DC, logic voltage: 3–5.5 V DC, I_{max} 2 A
Power supply	Meanwell LRS-350-24	24 V DC, 350 W, 14.6 A, 48–63 Hz
Control elements	Bigtreetech Manta M8P 2.0 Raspberry Pi CB4 1GB	STM32H723 550Mhz control board, two 4GB SD FLASH memory cards
Transmission mechanism	2 × 2GT 20 tooth gear, 2 × 2GT 60 tooth pinion 2 × 2GT-6 218 mm timing belt, 4 × 688ZZ bearings, 150 mm × 8 mm bar	Gear ratio 3:1
Software	Klipper	Control of the prototype can be realized using a Web interface with Wi-Fi protocol
3D printing materials	Creality PA12 white 1.75 mm	The print head elements are printed, A- and B-axis body

For the realization of additional axes, a PA12 nylon body (Fig. 5.4) has been printed, which was modified for use in cylindrical printing. For the realization of A and B axes, as in the 3-axis prototype, a reduction mechanism is used, which can be realized with 2GT 60-tooth and 20-tooth gears. An 8 mm diameter 150 mm long steel rod is used as a printing table, attached to a 2GT 60 teeth gear and a 668zz bearing. The gears are connected using a 218 mm 2GT

timing belt. The additional axis mechanism is mounted on the Y-axis printing table and can be screwed with M3 × 20 screws. The assembled mechanism is shown in Fig. 6.8.

Fig. 6.8. Additional A and B axis printing table mechanism from PA12 nylon material.

After creating the control code of the 5-axis prototype and assembling the prototype, it is necessary to calibrate the position of the final position sensors, placing the horizontal position of the A-axis so that the B-axis is placed horizontally to the printing table on the Y-axis. Next, the height of the print head is placed, and the Z-axis end position sensor is placed. All axis placement and prototype operation can be seen in Fig. 6.9.
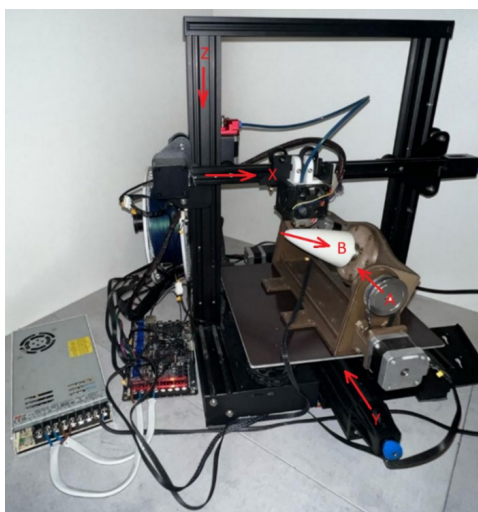
Fig. 6.9. 5-axis 3D printer prototype for the realization of non-layered cylindrical printing.

6.3. Conducting of experiments and summary of results

As a result, a 5-axis prototype for orthotic printing has been created, which uses a non-planar cylindrical printing method with a variable layer fill angle. An example is a printed finger orthosis using Creality PLA red sharp material. The manufactured orthosis has been compared with a traditional flat print orthosis of the same material printed using horizontal and vertical arrangement. According to the obtained results, the parameters of the obtained sample correspond to the parameters of cylindrical printing and it can be concluded that in a bending test compared to the horizontal sample, where the layers stick more due to adhesion, the non-

flat sample is up to 266 % stronger and is equivalent or up to 18 % stronger compared to vertical samples, yet the print quality is comparably better as no additional support material is required and the orthosis can be easily separated from the print base due to the use of an adhesive interlayer. As a result, no additional processing of the manufactured orthosis is required, and the surface quality is smooth and uniform (Fig. 6.10).

Fig. 6.10. 5-axis printed example of finger orthosis with a 45° layer infill.

CONCLUSIONS

1. The Thesis developed a non-random 3D printing method, which allows using the open and free traditional CAD model preparation methods that are already available for use now by manipulating 3D models and editing G-code generated by cutting programs. Thus, 3D printed objects with better parameters can be obtained, compared to traditional printing methods, faster without the use of support material, thus reducing the printing time.

2. The selection and mutual adjustment of components and components of FDM 3D printers play an important role because it directly affects the quality and accuracy of printing and can also make it possible to effectively use the potential of components, which leads to an increase in printing speed, and the efficient use of electricity leads to a reduction in electricity consumption.

3. The use of the traditional FDM 3D printing method for the production of individual orthopedic rehabilitation products is limited by the disadvantages of the traditional method, and cylindrical three-axis FDM 3D printing enables the production of individually tailored orthopedic rehabilitation products without the use of a support material, which leads to better surface quality and better mechanical properties of the manufactured product. However, the three-axis solution cannot effectively print complex shapes without a support material and is limited to simple orthotic shapes.

4. The five-axis FDM 3D cylindrical method can eliminate the shortcomings of the three-axis method and is completely adapted to the production of customized orthopedic rehabilitation devices. The developed method makes it possible to prepare a CAD model and create a 3D printer control G-code in an accessible form.

5. The developed FDM 3D printer prototype enables quick switching between traditional, three-axis cylindrical and five-axis cylindrical printing methods by changing the printer components, which enables one machine to be used for several tasks, effectively using personal time and the necessary printer installation space.

6. Based on the results of bending and impact tests, it was found that samples printed using cylindrical technology show up to 18 % higher strength compared to their counterparts in the direction of layer printing created by the traditional method and up to 266 % compared to samples whose layers are perpendicular to the printing direction. This confirms the hypothesis that cylindrical printing improves the mechanical properties of the products due to a tighter adhesion of the layers.

7. Implementation of modern software solutions and optimization of slicing algorithms can significantly reduce printing time and the amount of materials required for product creation. Using faster control panels in combination with more efficient stepper motor drivers can increase the print speed, reducing the total print time by up to 50 % when compared to samples printed using support material, yet reducing power consumption by an average of 2–3 % on a much larger microcontroller high-speed operations, increasing the efficiency of the 3D printing process.

8. Further research, including comparative analysis with traditional 3D printing methods, is needed to fully understand the energy benefits of cylindrical printing and non-planar slicing. It will help develop guidelines for reducing energy consumption in industry.

REFERENCES

[1] M. Vorobyov and I. Galkin, "Development and optimization of adjustable vibration source for investigation of prosthesis-to-human feedback of intellectual artificial limb: Simulation study," in *2014 IEEE 2nd Workshop on Advances in Information, Electronic and Electrical Engineering, AIEEE 2014 – Proceedings*, 2015. doi: 10.1109/AIEEE.2014.7020314.

[2] V. Vladinovskis, "Review of 3D Printing Technologies and Considerations on Their Use in Orthopedy," in *2020 IEEE 61th International Scientific Conference on Power and Electrical Engineering of Riga Technical University (RTUCON)*, 2020, pp. 1–6. doi: 10.1109/RTUCON51174.2020.9316483.

[3] S. A. Ashter, *Applications of Polymers and Plastics in Medical Devices: Design, Manufacture, and Performance*. in Plastics Design Library. Elsevier Science, 2022.

[4] P. Venezia, V. Ronsivalle, L. Rustico, E. Barbato, R. Leonardi, and A. Lo Giudice, "Accuracy of orthodontic models prototyped for clear aligners therapy: A 3D imaging analysis comparing different market segments 3D printing protocols," *J. Dent.*, vol. 124, 2022, doi: 10.1016/j.jdent.2022.104212.

[5] W. Leal Filho, A. M. Azul, L. Brandli, P. G. özuyar, and T. Wall, Eds., "Additive Manufacturing," in *Responsible Consumption and Production*, Cham: Springer International Publishing, 2020, p. 1. doi: 10.1007/978-3-319-95726-5_300002.

[6] A. Al Rashid, S. A. Khan, S. G. Al-Ghamdi, and M. Koç, "Additive manufacturing: Technology, applications, markets, and opportunities for the built environment," *Autom. Constr.*, vol. 118, p. 103268, 2020, doi: https://doi.org/10.1016/j.autcon.2020.103268.

[7] N. Shahrubudin, T. C. Lee, and R. Ramlan, "An Overview on 3D Printing Technology: Technological, Materials, and Applications," *Procedia Manuf.*, vol. 35, pp. 1286–1296, 2019, doi: https://doi.org/10.1016/j.promfg.2019.06.089.

[8] Y. Kewuyemi, H. Kesa, and O. Adebo, "Trends in functional food development with three-dimensional (3D) food printing technology: prospects for value-added traditionally processed food products," *Crit. Rev. Food. Sci. Nutr.*, vol. 62, pp. 1–38, May 2021, doi: 10.1080/10408398.2021.1920569.

[9] S. Bukhari, T. Tanveer, A. Abid, and S. Anwar, *Design and Fabrication of Inexpensive Portable Polar 3D Printer*. 2023. doi: 10.1109/ICRAI57502.2023.10089592.

[10] S. Singamneni, A. Roychoudhury, O. Diegel, and B. Huang, "Modeling and evaluation of curved layer fused deposition," *J. Mater. Process. Technol.*, vol. 212, no. 1, pp. 27–35, 2012, doi: https://doi.org/10.1016/j.jmatprotec.2011.08.001.

[11] J. Xu, X. Gu, D. Ding, Z. Pan, and K. Chen, "A review of slicing methods for directed energy deposition based additive manufacturing," *Rapid Prototyp. J.*, vol. 24, Oct. 2018, doi: 10.1108/RPJ-10-2017-0196.

[12] J. Jiang, X. Xu, and J. Stringer, "Support structures for additive manufacturing: A review," *Journal of Manufacturing and Materials Processing*, vol. 2, no. 4. MDPI, Dec. 01, 2018. doi: 10.3390/jmmp2040064.

[13] Y. Yang, J. Y. H. Fuh, H. T. Loh, and Y. S. Wong, "Multi-orientational deposition to minimize support in the layered manufacturing process," *J. Manuf. Syst.*, vol. 22, no. 2, pp. 116–129, 2003, doi: https://doi.org/10.1016/S0278-6125(03)90009-4.

[14] J. Xu, X. Gu, D. Ding, Z. Pan, and K. Chen, "A review of slicing methods for directed energy deposition based additive manufacturing," *Rapid Prototyping Journal*, vol. 24, no. 6. Emerald Group Holdings Ltd., pp. 1012–1025, Oct. 15, 2018. doi: 10.1108/RPJ-10-2017-0196.

[15] L. Meng *et al.*, "From topology optimization design to additive manufacturing: Today's success and Tomorrow's roadmap."

[16] W. Xiangping, Z. Haiou, W. Guilan, and W. Lingpeng, "Adaptive Slicing for Multi-axis Hybrid Plasma Deposition and Milling."

[17] M. Wüthrich, M. Gubser, W. J. Elspass, and C. Jaeger, "A novel slicing strategy to print overhangs without support material," *Applied Sciences (Switzerland)*, vol. 11, no. 18, Sep. 2021, doi: 10.3390/app11188760.

[18] B. Kumar Mawandiya, K. Pancholi, D. B. Shah, and S. J. Joshi, "Parametric study on process parameters of FDM 3D printer for thermoplastic materials," *Mater. Today Proc.*, vol. 59, pp. 373–378, 2022, doi: https://doi.org/10.1016/j.matpr.2021.10.504.

[19] "Motion Control, Solved. MOTOR ENGINEERING & MANUFACTURING." [Online]. Available: www.linengineering.com

[20] S. Baas and V. Saggiomo, "Ender3 3D printer kit transformed into open, programmable syringe pump set," *HardwareX*, vol. 10, 2021, doi: 10.1016/j.ohx.2021.e00219.

[21] K. F. Eichholz, I. Gonçalves, X. Barceló, A. S. Federici, D. A. Hoey, and D. J. Kelly, "How to design, develop and build a fully-integrated melt electrowriting 3D printer," *Addit. Manuf.*, vol. 58, p. 102998, 2022, doi: https://doi.org/10.1016/j.addma.2022.102998.

[22]   P. Venezia, V. Ronsivalle, L. Rustico, E. Barbato, R. Leonardi, and A. Lo Giudice, "Accuracy of orthodontic models prototyped for clear aligners therapy: A 3D imaging analysis comparing different market segments 3D printing protocols," *J. Dent.*, vol. 124, 2022, doi: 10.1016/j.jdent.2022.104212.

[23]   H. Ramaraju *et al.*, "Clinical grade manufacture of 3D printed patient-specific biodegradable devices for pediatric airway support," *Biomaterials*, vol. 289, 2022, doi: 10.1016/j.biomaterials.2022.121702.

[24]   R. Rogosic *et al.*, "Cost-effective, scalable and smartphone-controlled 3D-Printed syringe pump – From lab bench to point of care biosensing applications," *Physics in Medicine*, vol. 14, 2022, doi: 10.1016/j.phmed.2022.100051.

[25]   K. Reeser and A. L. Doiron, "Three-Dimensional Printing on a Rotating Cylindrical Mandrel: A Review of Additive-Lathe 3D Printing Technology," *3D Printing and Additive Manufacturing*, vol. 6, no. 6. Mary Ann Liebert Inc., pp. 293–307, Dec. 01, 2019. doi: 10.1089/3dp.2019.0058.

[26]   A. T. de Almeida, F. J. T. E. T. E. Ferreira, and J. A. C. Fong, "Standards for Efficiency of Electric Motors," *IEEE Industry Applications Magazine*, vol. 17, no. 1, pp. 12–19, 2011, doi: 10.1109/MIAS.2010.939427.

[27]   M. M. Hoque, M. M. H. Jony, M. M. Hasan, and M. H. Kabir, "Design and Implementation of an FDM Based 3D Printer," in *2019 International Conference on Computer, Communication, Chemical, Materials and Electronic Engineering (IC4ME2)*, 2019, pp. 1–5. doi: 10.1109/IC4ME247184.2019.9036538.

[28]   V. Vladinovskis, "Review of Lathe Type 3D Printers and Their Possible Improvements," in *2021 IEEE 9th Workshop on Advances in Information, Electronic and Electrical Engineering (AIEEE)*, 2021, pp. 1–5. doi: 10.1109/AIEEE54188.2021.9670257.

[29]   Y. Khan, "Characterizing the properties of tissue constructs for regenerative engineering," in *Encyclopedia of Biomedical Engineering*, vol. 1–3, Elsevier, 2019, pp. 537–545. doi: 10.1016/B978-0-12-801238-3.99897-0.

[30]   H. Farhat, "Chapter 3 – Materials and coating technologies," in *Operation, Maintenance, and Repair of Land-Based Gas Turbines*, H. Farhat, Ed., Elsevier, 2021, pp. 63–87. doi: https://doi.org/10.1016/B978-0-12-821834-1.00007-1.

[31]   British Standards Institution, *Plastics – Determination of flexural properties*. 2019.

[32]   H. Ullah and V. V Silberschmidt, "19 – Dynamic large-deflection bending of laminates," 2016, doi: 10.1016/B978-0-08-100870-6.00019-5.

[33]   V. Vladinovskis, "Selection of microcontroller board and stepper motor driver for FDM 3D printing to reduce power consumption."

[34]   C. G. Jones and C. Chen, "An arduino-based sensor to measure transendothelial electrical resistance," *Sens. Actuators A Phys.*, vol. 314, p. 112216, 2020, doi: https://doi.org/10.1016/j.sna.2020.112216.

[35]   G. Prachchhak, C. Bhatt, and J. Thik, "Data Logging and Visualization Using Bolt IoT," in *Advances in Intelligent Systems and Computing*, 2019, pp. 155–164. doi: 10.1007/978-981-13-2673-8_18.

[36]   "Fully Integrated, Hall Effect-Based Linear Current Sensor with 2.1 kVRMS Voltage Isolation and a Low-Resistance Current Conductor ACS712." [Online]. Available: www.allegromicro.com

[37]   V. Vladinovskis, "Potential Power Management Efficiency Improvements in Desktop 3D Printers," in *2022 IEEE 63rd International Scientific Conference on Power and Electrical Engineering of Riga Technical University (RTUCON)*, 2022, pp. 1–6. doi: 10.1109/RTUCON56726.2022.9978882.

[38]   M. S. Khan, "Effective and Precise Energy Meter," in *Lecture Notes in Networks and Systems*, 2022, pp. 795–802. doi: 10.1007/978-981-16-6407-6_68.

[39]   O. V Gnana Swathika, G. Kanimozhi, E. Umamaheswari, S. Rujay, and S. Saha, "IoT-Based Energy Management System with Data Logging Capability," in *Lecture Notes in Electrical Engineering*, 2021, pp. 547–555. doi: 10.1007/978-981-15-7241-8_41.

[40]   A. Sharma, S. Pal, P. Mahalle, B. A. Botre, and S. A. Akbar, "The development of current, speed and torque measurement system for low power electric vehicle motion control applications," in *AIP Conference Proceedings*, 2021. doi: 10.1063/5.0043937.

[41]   F. Galliana, R. Cerri, and D. Corona, "Automatic DC voltage precision resistive divider with ratios between 10:1 and 107:1," *Measurement*, vol. 183, p. 109865, 2021, doi: https://doi.org/10.1016/j.measurement.2021.109865.

[42]   Sean Aranda, *3D Printing Failures: 2022 Edition: How to Diagnose and Repair ALL Desktop 3D Printing Issues*, 2022 Edition. Independently published, 2021.

[43]   F. Hong, S. Hodges, C. Myant, and D. E. Boyle, "Open5x: Accessible 5-axis 3D printing and conformal slicing," in *Extended Abstracts of the 2022 CHI Conference on Human Factors in Computing Systems*, in CHI EA '22. New York, NY, USA: Association for Computing Machinery, 2022. doi: 10.1145/3491101.3519782.

[44]   A. Dine and G.-C. Vosniakos, "On the development of a robot-operated 3D-printer," *Procedia Manuf.*, vol. 17, pp. 6–13, 2018, doi: https://doi.org/10.1016/j.promfg.2018.10.004.

Vlads Vladinovskis

RESEARCH AND DEVELOPMENT OF 3D PRINTING EQUIPMENT FOR THE MANUFACTURE OF ORTHOPEDIC REHABILITATION PRODUCTS

Summary of the Doctoral Thesis

Vlads Vladinovskis was born in 1995 in Daugavpils. He obtained a Bachelor's degree in Electrical Engineering (2018) and a Professional Master's degree and electrical engineer's qualification (2020) from Riga Technical University (RTU). Since 2021, he has been working at Riga Technical University, holding the position of scientific assistant. His scientific interests are related to 3D printing technologies, computer science and control systems of controllers, microcontrollers and microprocessors.